NASA-CR-72607

SRI Project PMD 7359

THE EFFECT OF SILICON AND MANGANESE ON THE OXIDATION OF Ni-20Cr AND Co-20Cr ALLOYS

by

D. L. Douglass

STANFORD RESEARCH INSTITUTE

prepared for

NATIONAL AERONAUTICS AND SPACE ADMINISTRATION

NASA Lewis Research Center

Contract NAS 3-11165

Fredric H. Harf, Project Manager

Carl E. Lowell, Research Advisor

NOTICE

This report was prepared as an account of Government-sponsored work. Neither the United States, nor the National Aeronautics and Space Administration (NASA), nor any person acting on behalf of NASA:

A. Makes any warranty or representation, expressed or implied, with respect to the accuracy, completeness, or usefulness of the information contained in this report, or that the use of any information, apparatus, method, or process disclosed in this report may not infringe privately-owned rights; or

B. Assumes any liabilities with respect to the use of, or for damages resulting from the use of, any information, apparatus, method or process disclosed in this report.

As used above, "person acting on behalf of NASA" includes any employee of such contractor, to the extent that such employee or contract of NASA or employee of such contractor prepares, disseminates, or provides access to any information pursuant to his employment or contract with NASA, or his employment with such contractor.

Requests for copies of this report should be referred to:

National Aeronautics and Space Administration
Scientific and Technical Information Facility
P. O. Box 33
College Park, Maryland 20740

NASA-CR- 72607

SRI Project PMD 7359

TOPICAL REPORT

THE EFFECT OF SILICON AND MANGANESE ON THE OXIDATION OF Ni-20Cr and Co-20Cr ALLOYS

by

D. L. Douglass

STANFORD RESEARCH INSTITUTE

Menlo Park, California 94025

prepared for

NATIONAL AERONAUTICS AND SPACE ADMINISTRATION

May 1969

CONTRACT NAS 3-11165

NASA Lewis Research Center
Cleveland, Ohio

Fredric H. Harf, Project Manager
Carl E. Lowell, Research Advisor

Materials and Structures Division

ABSTRACT

Additions of 3% silicon or manganese to Ni-20Cr reduced the oxidation rate, whereas, additions of 1% had little effect. Three percent silicon alloys formed an inner scale of SiO_2, and three percent manganese alloys formed an inner spinel layer of essentially pure $MnCr_2O_4$. The experimentally determined solid-state growth rate[8] of $NiCr_2O_4$ was about 1000 times slower than the growth rate for Cr_2O_3. It has been established that the protective layer on Ni-20Cr (Nichrome alloys) is the spinel and not Cr_2O_3 as previously postulated. Similar measurements for the growth of $CoCr_2O_4$ showed that Cr_2O_3 is the protective layer on Co-20Cr. Mechanisms for scale growth are given for both Ni-20Cr and Co-20Cr alloys.

CONTENTS

ILLUSTRATIONS

ILLUSTRATIONS (Continued)

ILLUSTRATIONS (Concluded)

SUMMARY

Contrary to earlier studies, it has been found that spinel layers offer more protection against oxidation than Cr_2O_3 films on Ni-20Cr when the spinel exists between the alloy and the Cr_2O_3. The rates of formation of such a layer are about 1000 times slower than the rate of formation of Cr_2O_3. An outer spinel layer also exists but offers little protection. The outer layer forms by reaction of the couple $NiO-Cr_2O_3$, the NiO being the first oxide to form, and the Cr_2O_3 the second. The rate-controlling step is the diffusion of chromium in NiO. The thin layer of NiO permits a build-up of chromium to the solubility limit, followed by spinel formation. The outer spinel readily spalls off.

Manganese additions (particularly 3%) reduce the oxidation rate by enabling a tenaciously bound inner spinel to form which is essentially $MnCr_2O_4$.

Silicon additions also reduce the oxidation rate by means of a layer of silica (alpha-cristobalite) that forms at the oxide-metal interface. Discontinuous layers formed in alloys containing 1% silicon, whereas nearly continuous layers existed in alloys containing 3% silicon. The outer layers were highly susceptible to spalling upon cooling.

Spinel layers in the scales of Co-20Cr alloys were less protective than layers of Cr_2O_3. The CoO formed very rapidly initially and subsequently reacted with Cr_2O_3, which formed at a later stage. The large mass of CoO that existed, as well as the much more rapid rate of $CoCr_2O_4$ formation compared to the rate of Cr_2O_3 growth, resulted in the Cr_2O_3 being used up faster than it formed. This behavior was opposite that observed in Ni-Cr alloys.

Manganese additions slightly reduced the oxidation rate, as well as the solid-state growth rate of spinel. However, the spinel still formed faster than new Cr_2O_3, and hence the protective layer of Cr_2O_3 was used up.

Silicon additions reduced the oxidation rate, but the layers were highly susceptible to spalling upon cooling as well as during isothermal oxidation. The scales contained both spinel and Co_2SiO_4. The orthosilicate was present as isolated particles and did not offer a continuous protective film per se. The reduced oxidation rate was associated with a thin inner film of Cr_2O_3.

INTRODUCTION

Commercial, high temperature, oxidation resistant alloys are generally either nickel or cobalt base and contain 10 to 20% chromium. The chromium is added primarily to impart oxidation resistance. Nearly all nickel and cobalt alloys contain small amounts of both silicon and manganese as residual impurities, the amounts usually ranging from about 0.5 to 2%. Although the oxidation behavior of the binary alloys Ni-20Cr and Co-20Cr, which are the starting compositions to which other additions are made, is well known, the effects of the impurities are poorly defined.

Hickman and Gulbransen[1] observed a sixfold increase in the lifetime of Nichrome-type heating elements as the manganese content was lowered from 1.70 to 0.01% and the silicon content was raised from 0.3 to 1.39%. Crystal structure studies of films formed on the alloys showed that the low manganese-high silicon alloy formed Cr_2O_3 predominantly but that the high manganese-low silicon alloy formed a significant amount of $MnCr_2O_4$ spinel in addition to NiO and Cr_2O_3. The shorter lifetime and poorer oxidation resistance of the high manganese alloy were associated with the presence of the manganese spinel. High manganese contents were not necessarily detrimental if sufficient amounts of silicon were present to counteract the effect of manganese.

Sugiyama and Nakayama[2] examined the scales formed by oxidation of Nichrome containing from 0.5 to 1.5% silicon over the range of 700 to 900°C. No evidence of silica was found in the scales that had been stripped from the metal. However, heating of these scales at 1200°C for three hours resulted in the presence of alpha-cristobalite in the X-ray pattern. Their interpretation of these results was that amorphous silica formed during oxidation but that it crystallized upon heating at a temperature higher than that of the oxidation run. The scales generally consisted of Cr_2O_3 and spinels.

Subsequent work by Gulbransen and coworkers[3,4] was performed in order to define the role of both silicon and manganese in the oxidation behavior of Nichrome-type heater alloys. Most of their data were obtained at "low" temperatures in the range of 400 to 900°C (although a few runs were made at temperatures up to 1100°C) and for short times of up to about 400 minutes. Several interesting observations were made, but they concluded that the exact role of these elements was still unknown.

EXPERIMENTAL PROCEDURES

Sample Preparation

High-purity nickel(99.97%), chromium (99.95%), and cobalt (99.9%) were used for the base alloys; silicon (99.99%) and manganese (99.0%) were added. Two hundred gram buttons were triple arc-melted on a water-cooled copper hearth in an inert arc furnace. The buttons were turned over before each remelt. The argon atmosphere was gettered by melting a zinconium button and allowing it to react with residual oxygen and nitrogen.

The buttons were hot-rolled at 950°C to 20-mil sheet (for six of the alloys), which was sand-blasted to remove surface oxides. The hot-rolled sheet was cold-rolled to 11-mil sheet and vacuum-annealed for one hour at 950°C. The other four alloys were hot-rolled at 950°C to 50-mil sheet, sand-blasted, cold-rolled to 30-mil sheet, and vacuum-annealed as above. Chemical analyses of the alloys are listed in Table I.

Oxidation samples were sheared and drilled, re-annealed, and electropolished in a solution of 60% H_3PO_4-40% H_2SO_4 containing 10 gm CrO_3/liter. The samples were rinsed, dried, and weighed and measured.

Oxidation Tests

Thermogravimetric tests were performed mostly in the Cahn recording microbalance shown schematically in Fig. 1. Because of the small sample size and the high sensitivity of the balance, convection currents markedly affected the results and so it was necessary to perform the oxidation tests in a closed system at an oxygen partial pressure of 0.21 atm.

A few of the samples were tested by making continuous measurements in air on a bottom-weigh Ainsworth balance mounted above a vertical furnace. Larger samples could be measured by this method than in the Cahn balance.

Table I

CHEMICAL ANALYSES OF ALLOYS

Alloy Designation	Percent by Weight*				
	Cr	Si	Mn	Ni	Co
Ni-20Cr	19.28	0.034		Balance	-
	19.27	0.016	0.001		
Ni-20Cr-1Mn	19.17	0.047	0.99	Balance	-
	19.17	0.062	0.81		
Ni-20Cr-3Mn	19.15	0.100	2.85	Balance	-
	19.10	0.055	2.78		
Ni-20Cr-1Si	19.18	1.07		Balance	-
	19.18	0.89	0.001		
Ni-20Cr-3Si	18.90	2.91	0.006	Balance	-
	18.97	2.81			
Co-20Cr	19.45	0.031	0.036	-	Balance
	19.41	0.014			
Co-20Cr-1Mn	19.54	0.024	0.82	-	Balance
	19.62	0.019	0.75		
Co-20Cr-3Mn	19.13	0.029	2.41	-	Balance
	19.17	0.021	2.48		
Co-20Cr-1Si	19.73	0.93	0.01		Balance
	19.72	0.88			
Co-20Cr-3Si	19.52	2.99	0.126		Balance
	19.48	2.90	0.100		

*Duplicate analyses.

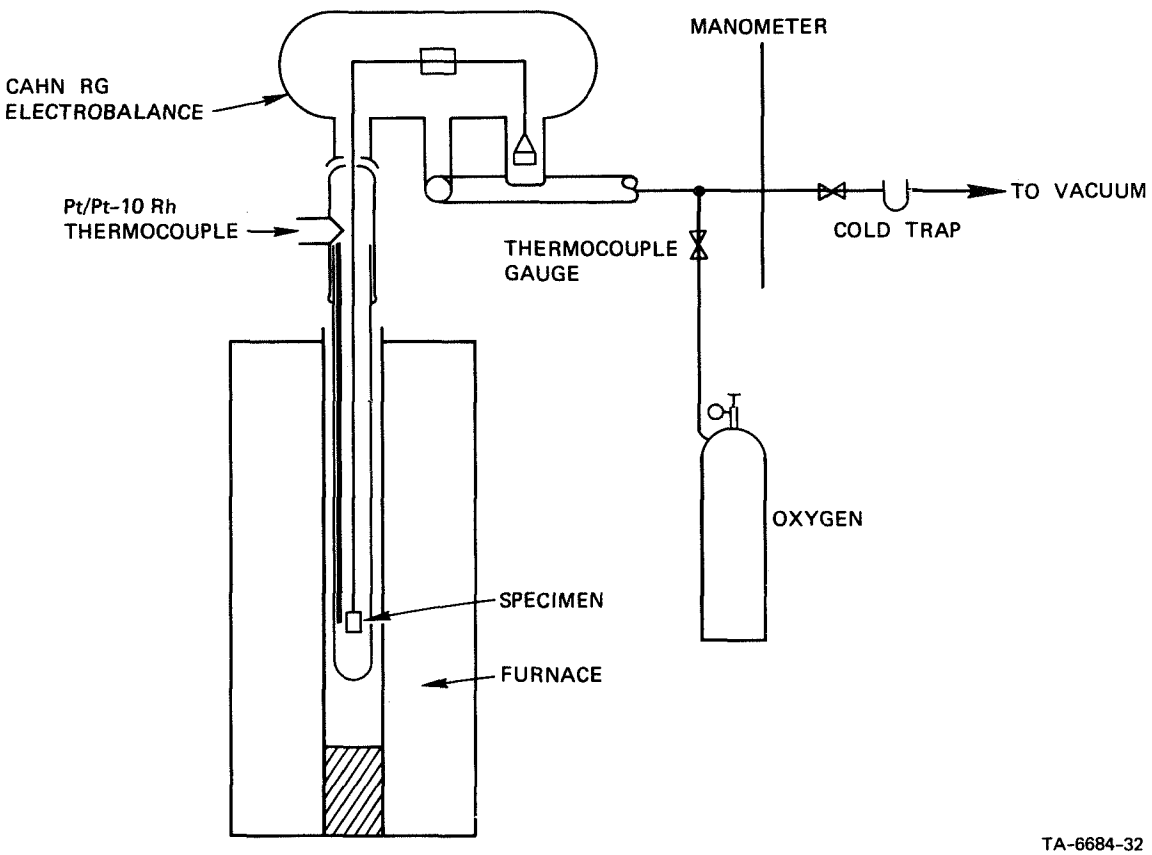

FIGURE 1 SCHEMATIC DIAGRAM OF CAHN THERMOGRAVIMETRIC APPARATUS

Analyses of Oxide Films

Conventional metallographic, X-ray diffraction, and electron microprobe techniques were employed to characterize the oxides formed. One nonconventional technique was also used for X-ray diffraction. This consisted of dissolving the metal substrate of the alloys in a solution of ethyl acetate with 10% bromine at 75°C. The oxides were not attacked and were collected, cleaned, and subjected to various diffraction tests. This technique was particularly useful for identifying those oxides that did not spall from the sample. Spalled oxides were simply collected and subjected to a Debye-Scherrer analysis.

RESULTS

Thermogravimetric Analyses

The kinetics of oxidation were determined by measuring weight change as a function of time. These measurements are shown in Figs. 2-9 on log-log plots. It must be emphasized that these plots are used solely to portray a wide range of times. There is no connection between a given slope on the log-log plot and any of the accepted rate laws. The reasons for this are the extreme hetrogeneity of the oxide layers and the fact that numerous oxides form; hence any attempts to assign rate laws to these curves is inherently wrong. Previous data appearing in the literature do not follow the parabolic rate law.

The kinetics curves for the cobalt alloys indicate that considerable spalling occurred during isothermal oxidation; thus it is difficult to make comparisons between the various alloys other than during the initial stages, which were well behaved. The addition of silicon to Co-20Cr appeared to be beneficial at the higher temperatures, e.g., 1200°C, in that the weight gains at any given time were considerably lower than for the undoped or manganese-containing alloys. The alloy with 1% silicon spalled during the isothermal oxidation, and both alloys spalled extensively during cooling.

The same problem existed for some of the nickel-base alloys, depending upon temperature and type of sample. For example, large samples having a surface area of about 0.1 to 0.2 dm^2 did not spall or spalled to a minor extent. On the other hand, the small samples having surface areas of about 0.03 to 0.05 dm^2 spalled extensively at temperatures below 1200°C. Spalling was associated with the "edge effect," which of course was more prevalent in the small samples. The oxide films were generally sufficiently plastic at 1200°C to deform and to relieve the stresses. Ni-20Cr-3Si spalled slightly after long times at 1200°C.

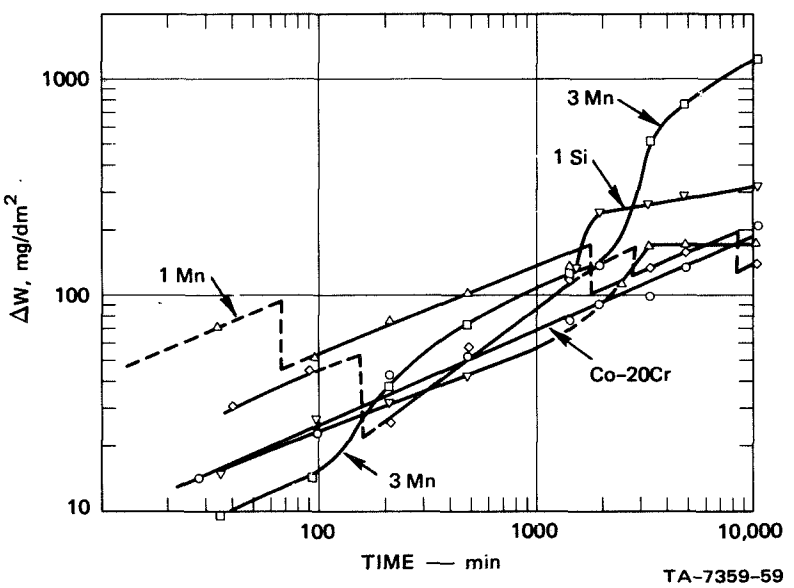

FIGURE 2 ISOTHERMAL OXIDATION OF Co-20Cr ALLOYS AT 1100°C

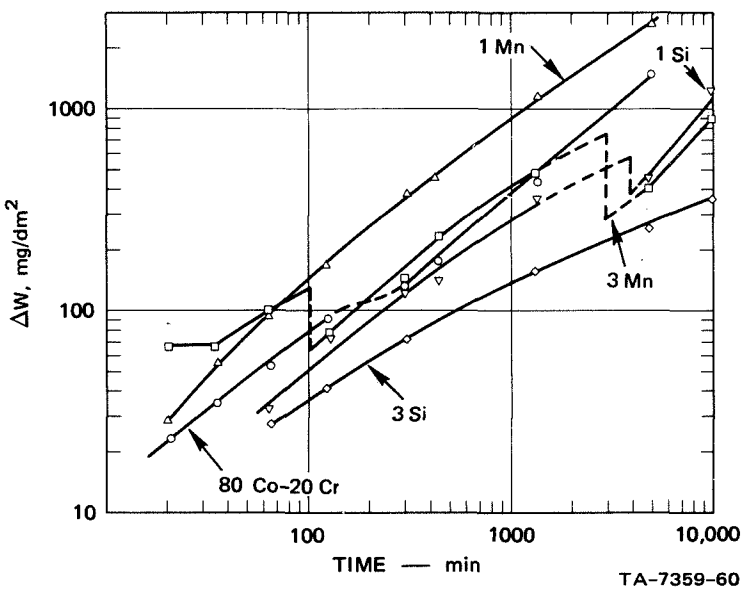

FIGURE 3 ISOTHERMAL OXIDATION OF Co-20Cr ALLOYS AT 1200°C

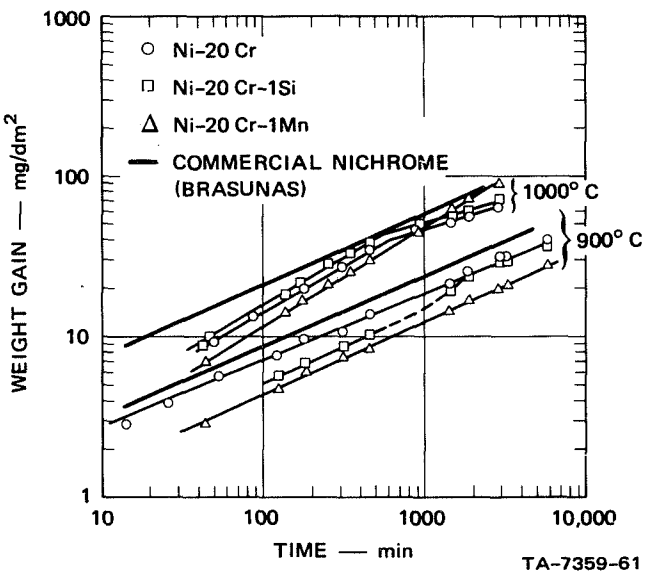

FIGURE 4 ISOTHERMAL OXIDATION OF VACUUM-ANNEALED Ni-20Cr ALLOYS (Large Samples, A ≈ 0.2 dm^2)

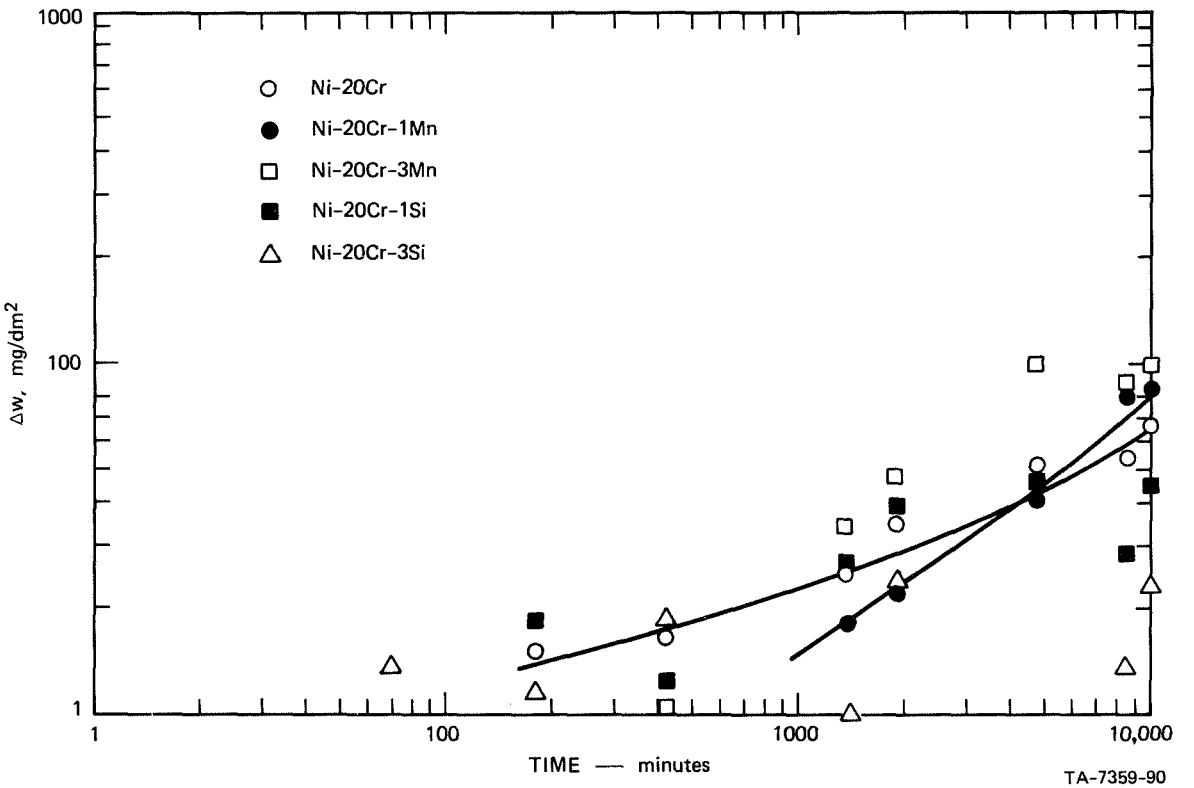

FIGURE 5 ISOTHERMAL OXIDATION OF Ni-20Cr ALLOYS AT 1000°C

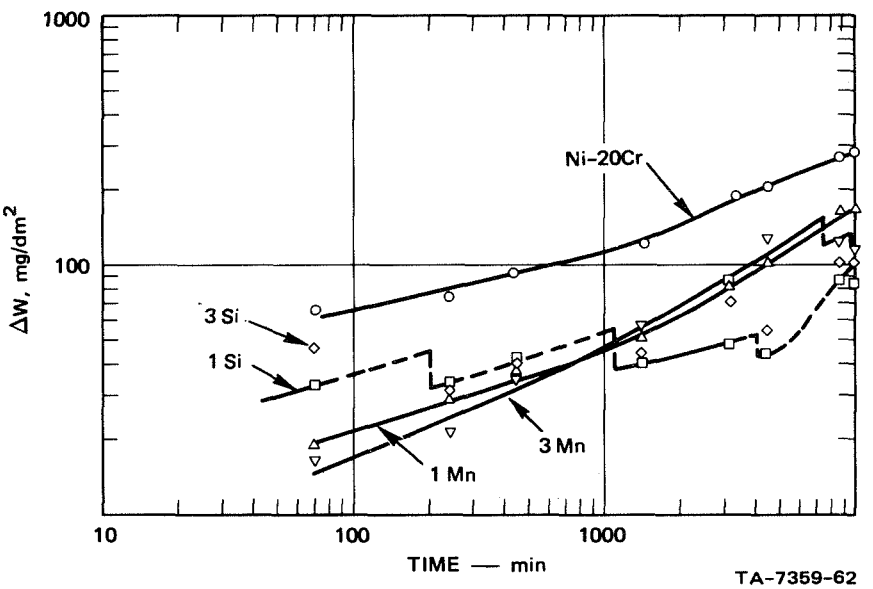

FIGURE 6 ISOTHERMAL OXIDATION OF Ni-20Cr ALLOYS AT 1100°C

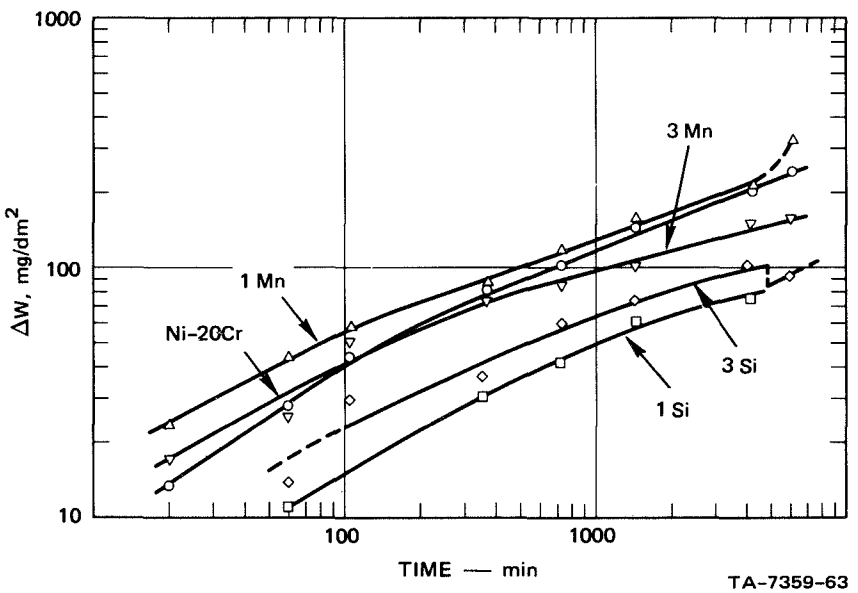

FIGURE 7 ISOTHERMAL OXIDATION OF Ni-20Cr ALLOYS AT 1200°C

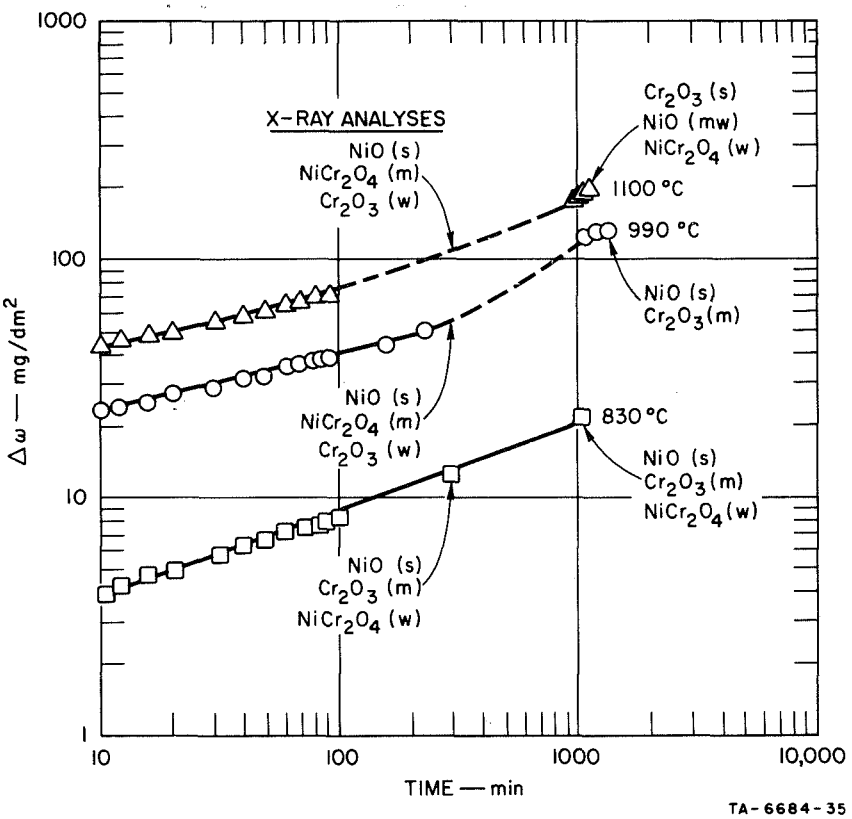

FIGURE 8 OXIDATION BEHAVIOR OF Ni-20Cr
s = strong, m = medium, w = weak

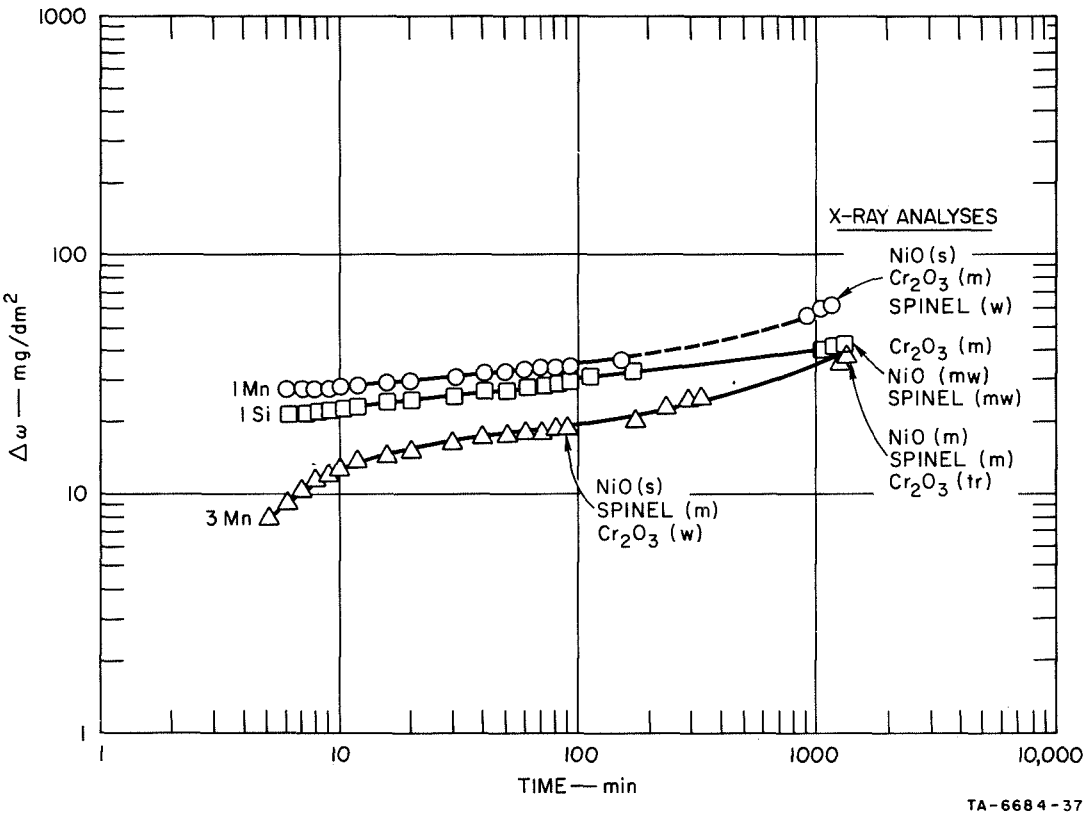

FIGURE 9 OXIDATION BEHAVIOR OF MANGANESE- AND SILICON-DOPED Ni-20Cr AT 970°C s = strong, m = medium, w = weak, tr = trace

The 1200°C data indicate that the addition of silicon to Ni-20Cr reduces the oxidation rate. It appears that at 1100°C manganese reduces the rate, although both alloys containing manganese spalled at this temperature, and it is possible that spalling at the earliest stages may have occurred. If this happened, the conclusion that manganese reduces the oxidation rate would be wrong. In other words, the spalling problem is sufficiently severe that the data at 1000° and 1100°C are suspect, and it is dangerous to make any firm conclusions. Also, as will be shown subsequently, the films are very hetrogenous, and it is not even possible to discern which films were the thickest.

The effect of temperature on the oxidation of Ni-20Cr is shown in Fig. 8. These data were obtained on small samples, and for some unknown reason no spalling occurred on any of the three samples. X-ray analyses of the oxides were made at various times and are indicated on the plots.

The effects of silicon and manganese at a given temperature are compared in Fig. 9. Since none of these samples exhibited spalling, it can be concluded that alloys containing silicon oxidize less during the early states than do alloys containing manganese. All the alloys were characterized by very rapid weight gains almost immediately upon exposure to the oxidizing environment followed by a very low rate of change. The films that formed did so rapidly and were then protective.

Metallography and Electron Microprobe Analyses

Cobalt Alloys

The scales formed on the cobalt-base alloys were extremely heterogeneous and were dependent upon both the location on the sample and the temperature. A macrograph of the "dogbone" type of scale is shown in Fig. 10. For example, at high temperatures, the flat parts of the samples oxidized to form thin, compact scales (Fig. 11a), but the ends formed extremely thick scales with an inner portion that appeared to be porous (Fig. 11b). The outer portion of the ends was CoO, and the inner portion was a mixture of CoO, spinel, and cobalt silicate on alloys containing silicon. The outer portion of CoO on the alloys containing manganese also contained a manganese-rich phase (the light portion in Fig. 11).

Similar structures are shown in Figs. 12 and 13 for Co-20Cr and Co-20Cr-1Mn respectively. The only significant difference between the scales on Co-20Cr-1Mn and those formed on Co-20Cr-3Mn is the absence of the manganese-rich phase in the CoO in the former. Apparently the critical manganese content for precipitation of this phase is between 1 and 3% Mn, which probably represents the solubility limit for manganese in CoO that contains some chromium in solution.

The scales on Co-20Cr-1Si were basically the same as the thick, duplex scales on Co-20Cr and the alloys containing manganese. An exception in the former was the presence of cobalt silicate, which is clearly seen in Fig. 14 as dark particles slightly below the outer CoO portion. On the other hand, the alloy containing 3% silicon exhibited three types of scales. The first type was similar to the thick duplex scales formed on the other alloys except that the formation of the outer CoO layer was definitely retarded. The second type (Fig. 15a) was a highly undulating, thin film. Large ridges formed during oxidation, and the scale tended to follow the ridges but was not tightly adherent. These alloys spalled extensively; thus there is the

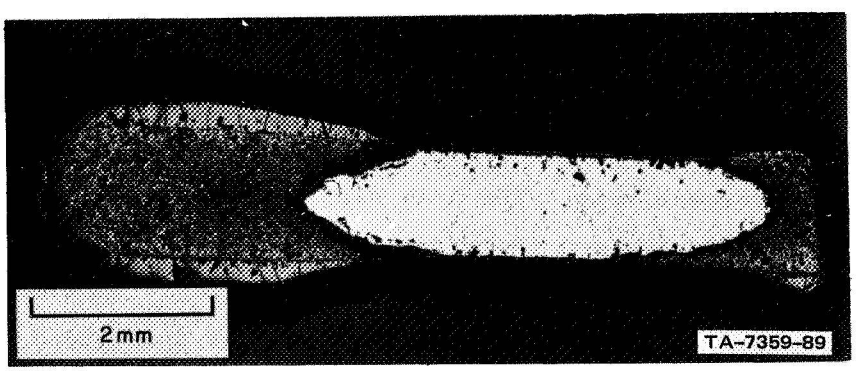

FIGURE 10 MACROGRAPH OF Co-20Cr-3Mn OXIDIZED 1 WEEK AT 1100°C SHOWING HETROGENEOUS NATURE OF SCALE ("Dogbone" Structure)

(a) THIN, COMPACT PORTION FROM FLAT SURFACE

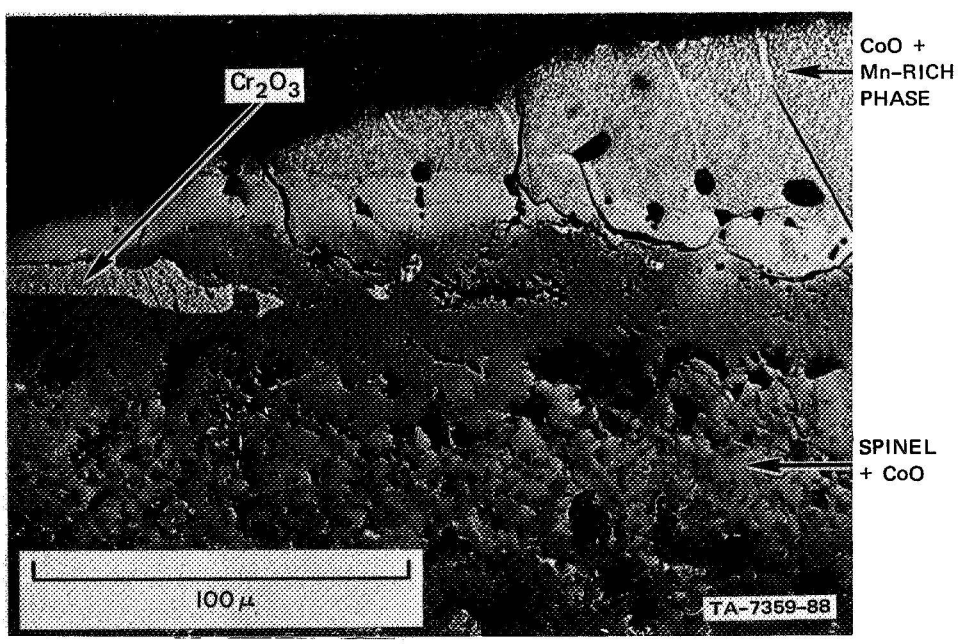

(b) THICK, DUPLEX PORTION AT ENDS

FIGURE 11 MICROGRAPHS OF SCALE FORMED ON SAMPLE SHOWN IN FIGURE 10 (Co-20Cr-3Mn oxidized 1 week at 1100°C)

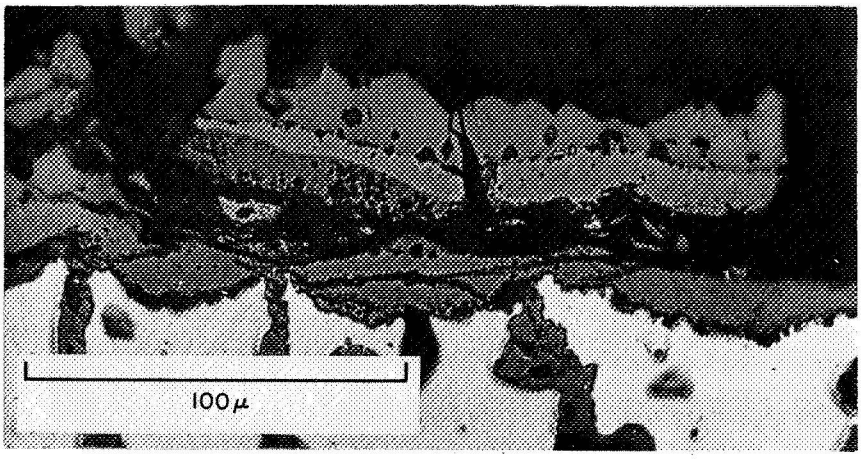

(a) THIN, COMPACT PORTION FROM FLAT SURFACES

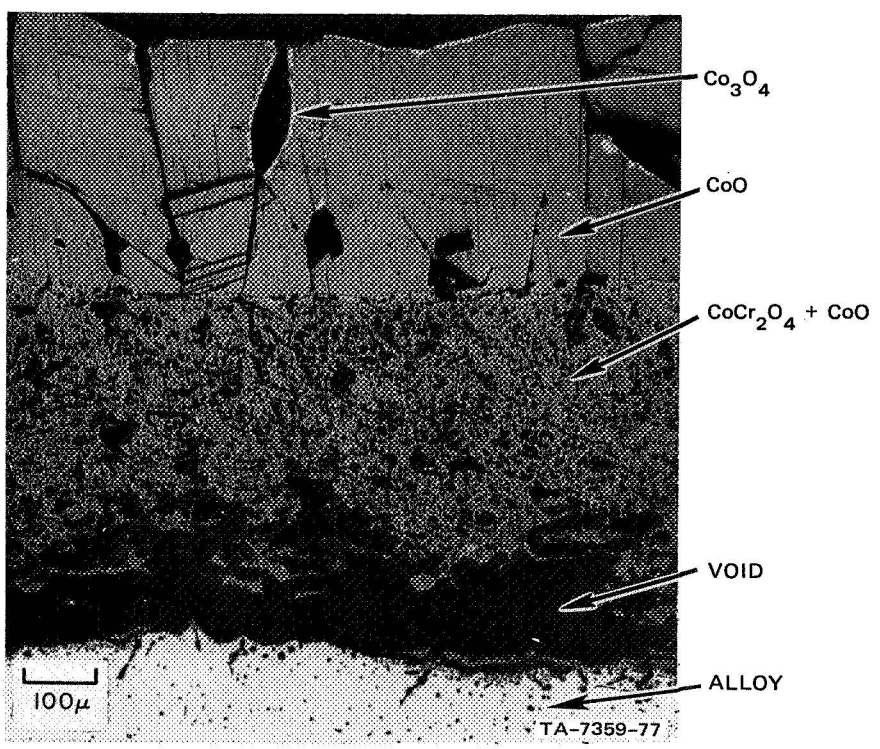

(b) THICK, DUPLEX PORTION AT ENDS

FIGURE 12 MICROGRAPHS OF SCALES FORMED ON Co-20Cr OXIDIZED FOR 2 WEEKS AT 1200°C

(a) THIN, COMPACT PORTION FROM FLAT SURFACE

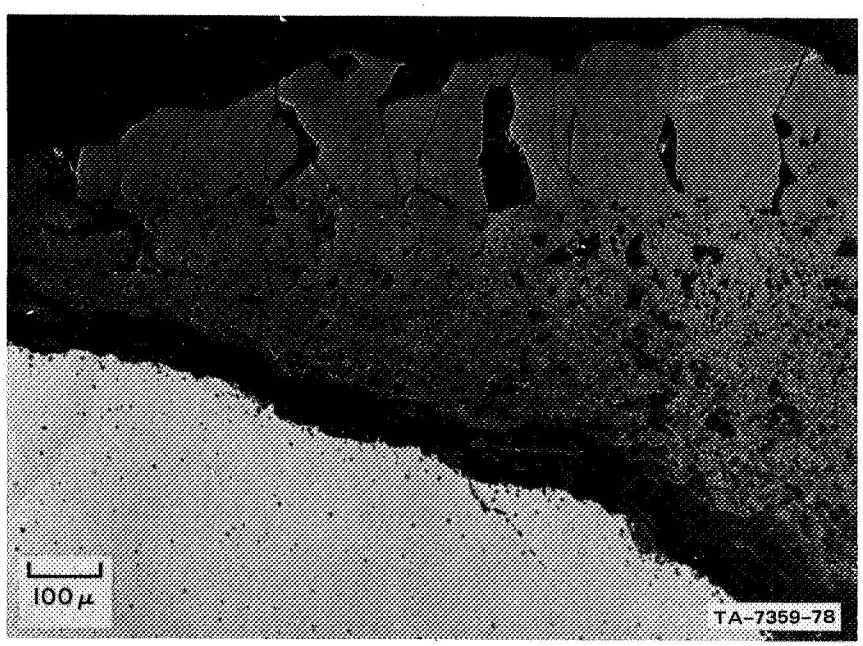

(b) THICK, DUPLEX PORTION AT ENDS

FIGURE 13 MICROGRAPHS OF SCALES FORMED ON Co-20Cr-1Mn OXIDIZED FOR (a) 1 Week at 1200°C and (b) 1 Week at 1100°C

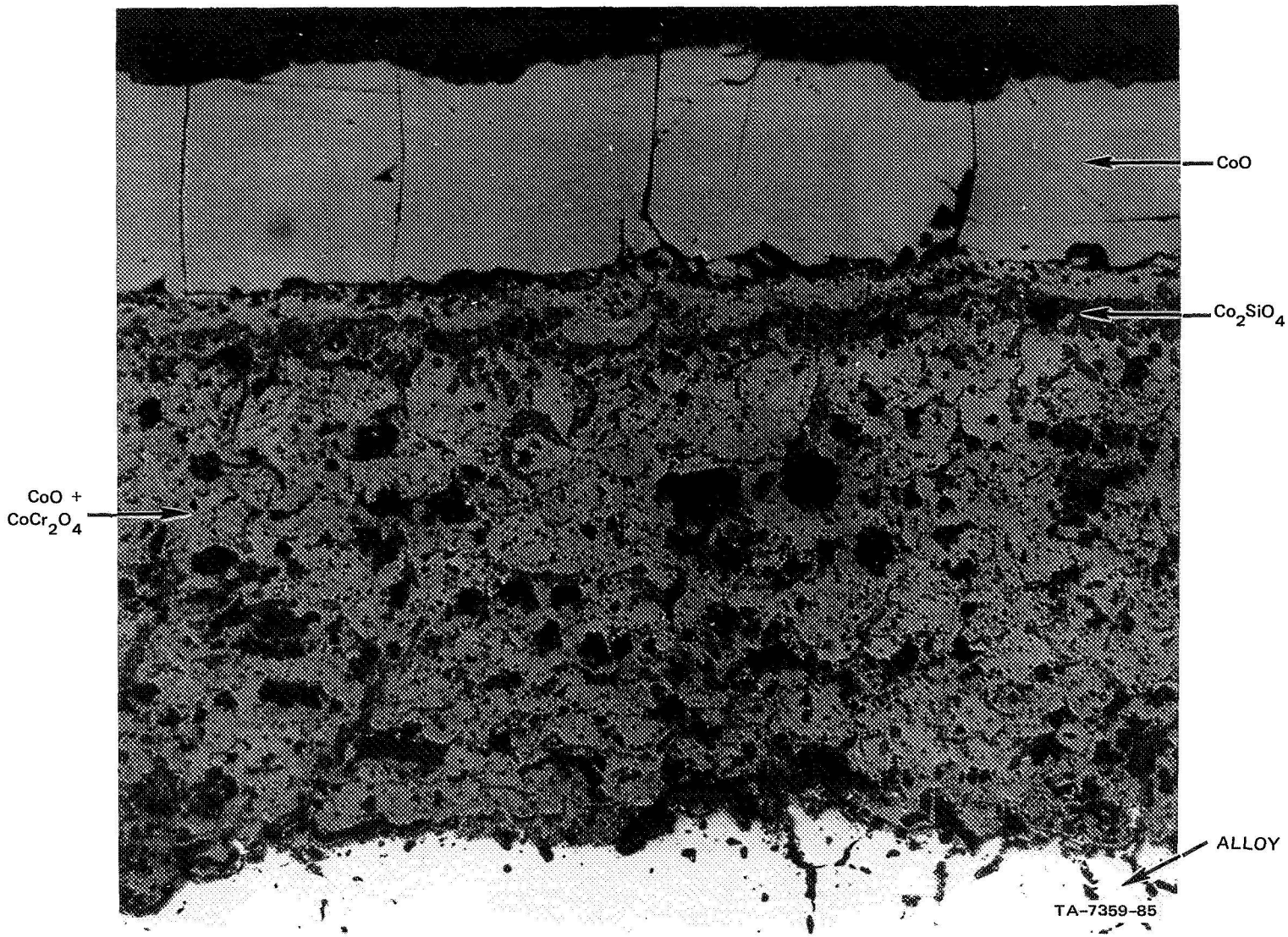

FIGURE 14 SCALE FORMED ON Co-20Cr-1Si OXIDIZED 2 WEEKS AT 1200°C

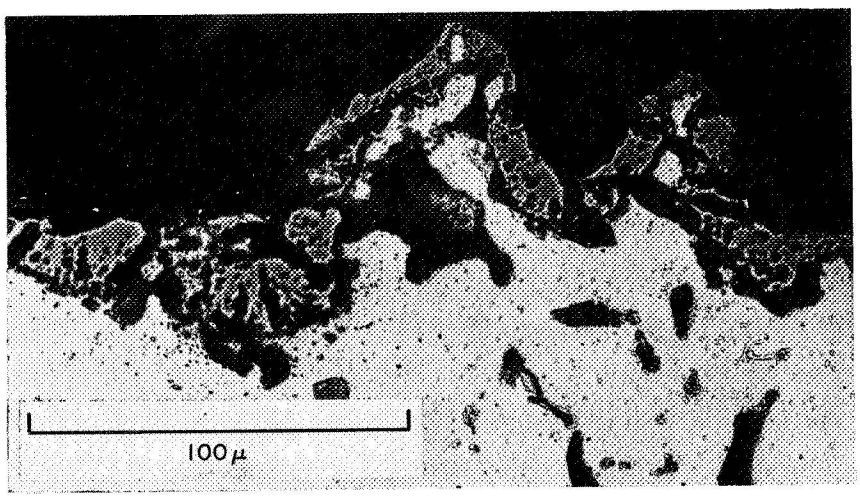

(a) EXAMPLE OF HIGHLY IRREGULAR SCALE SHOWING "UNDULATING" MORPHOLOGY. Oxidized 3 weeks at 1100° C.

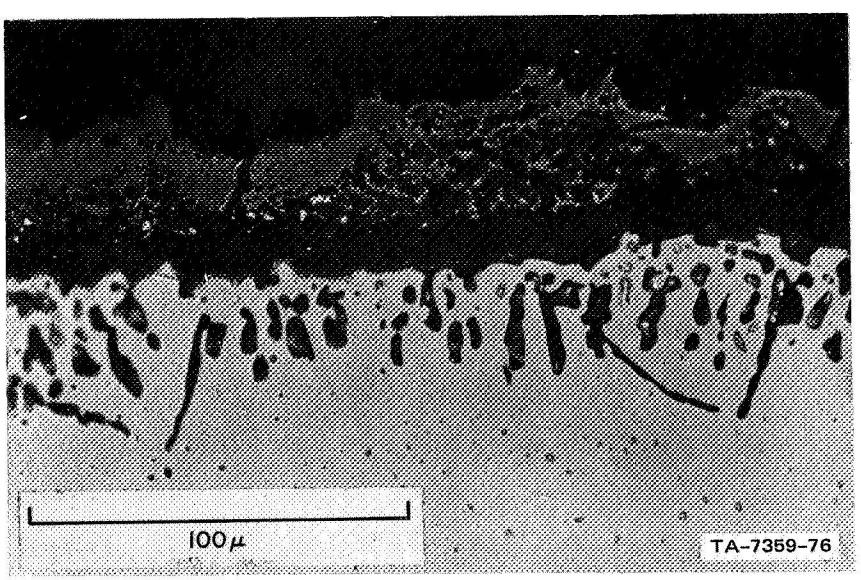

(b) UNIFORM SCALE SHOWING INTERNAL OXIDATION. Oxidized 1 week at 1200° C.

FIGURE 15 VARIOUS TYPES OF SCALES FORMED ON Co-20Cr-3Si

possibility that the scale shown in Fig. 15a was an inner layer which was the sole remnant of thicker scale, most of which was lost. The third type, Fig. 15b was much more uniform than the type -2 and also involved an internal oxide below the scale which was identified as Co_2SiO_4.

The results of electron microprobe analyses are shown as composite X-ray images along with the backscattered electron image micrographs in Fig. 16-19. Three of the composites are for the thick duplex layers and one is of a compact layer. The duplex layer on Co-20Cr consists of an outer CoO zone which is very dense and which contains comparatively little chromium in solution. As will be shown subsequently, this behavior is quite different from that of the nickel alloys. The inner portion of the duplex layer is two-phase, a mixture of CoO and the spinel, $CoCr_2O_4$. Both the micrographs and the backscattered electron image picture show much porosity. However, certain areas of the two-phase zone are fully dense, and it is strongly thought that the apparent porosity was created during metallographic polishing rather than during oxidation.

The duplex region of the scales that formed on the alloys containing silicon had cobalt silicate present, as well as CoO and $CoCr_2O_4$. There was also a silicon-rich phase at the extreme outside (at the CoO outer extremity). This phase appeared to be pure silica in the scale of Co-20Cr-1Si, as can be seen by the lack of cobalt in this area (Fig. 18).

The compact layer shown in Fig. 19 was also duplex, consisting of an inner Cr_2O_3 film under a Co-Mn-Cr spinel. A line traverse of this scale is given in Fig. 20. The base alloy, Co-20Cr, formed a similar scale, except that no manganese existed (Figs. 12a and 21). The outer CoO spalled off most of the samples. The line traverse of the Co-20Cr alloy scale revealed only the Cr_2O_3 inner zone and an outer zone of

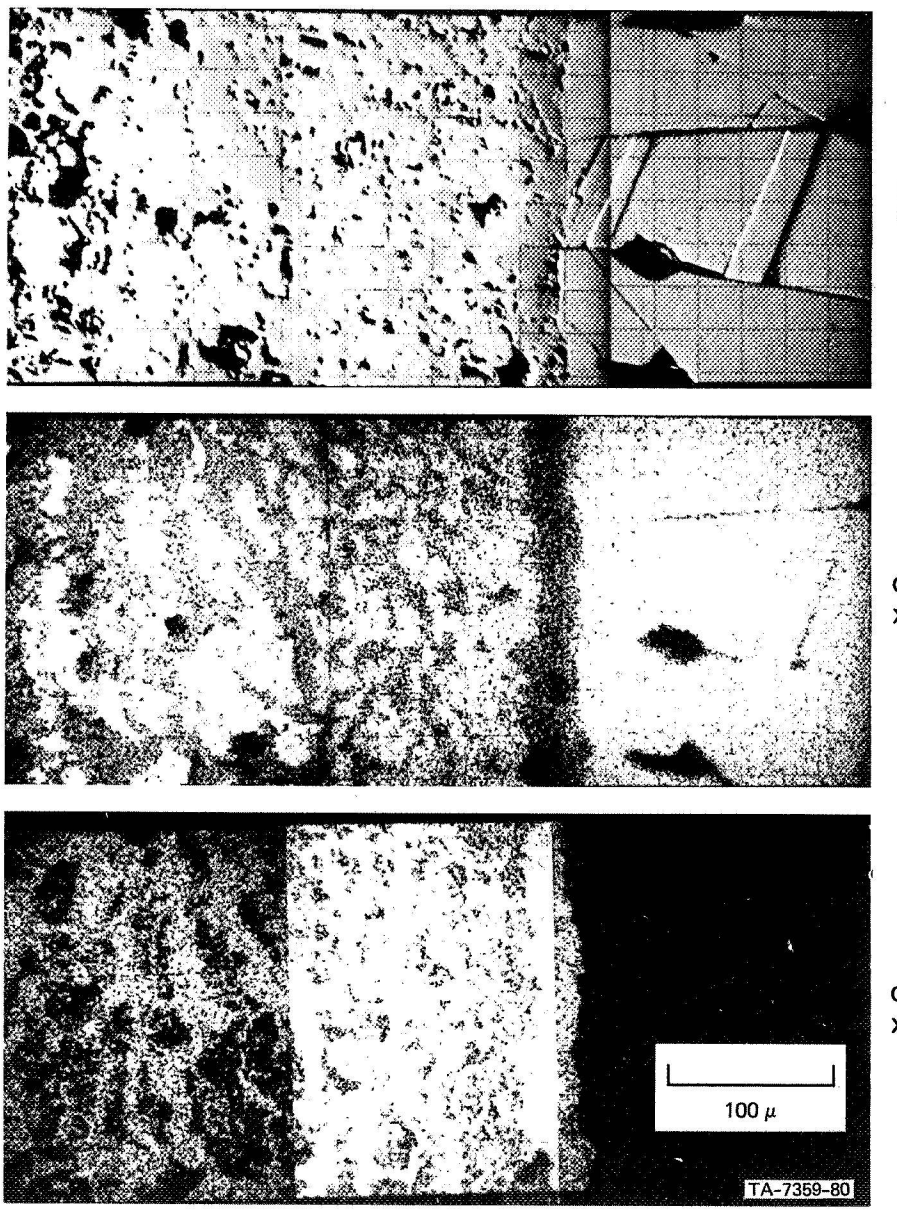

FIGURE 16 ELECTRON MICROPROBE ANALYSIS OF SCALE FORMED ON Co-20Cr OXIDIZED 2 WEEKS AT 1200°C

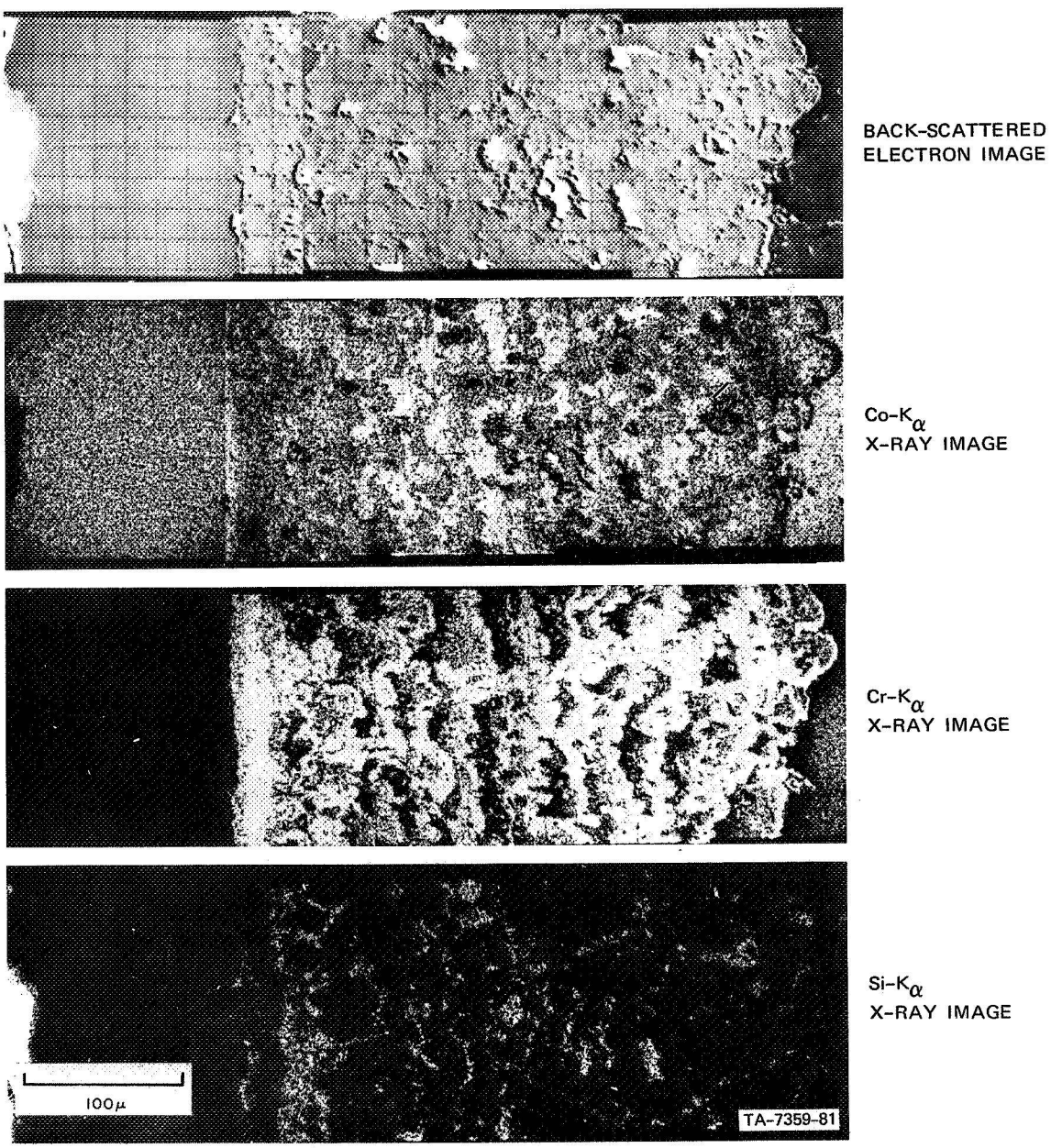

FIGURE 17 ELECTRON MICROPROBE ANALYSIS OF SCALE FORMED ON Co-20Cr-1Si OXIDIZED 2 WEEKS AT 1200°C

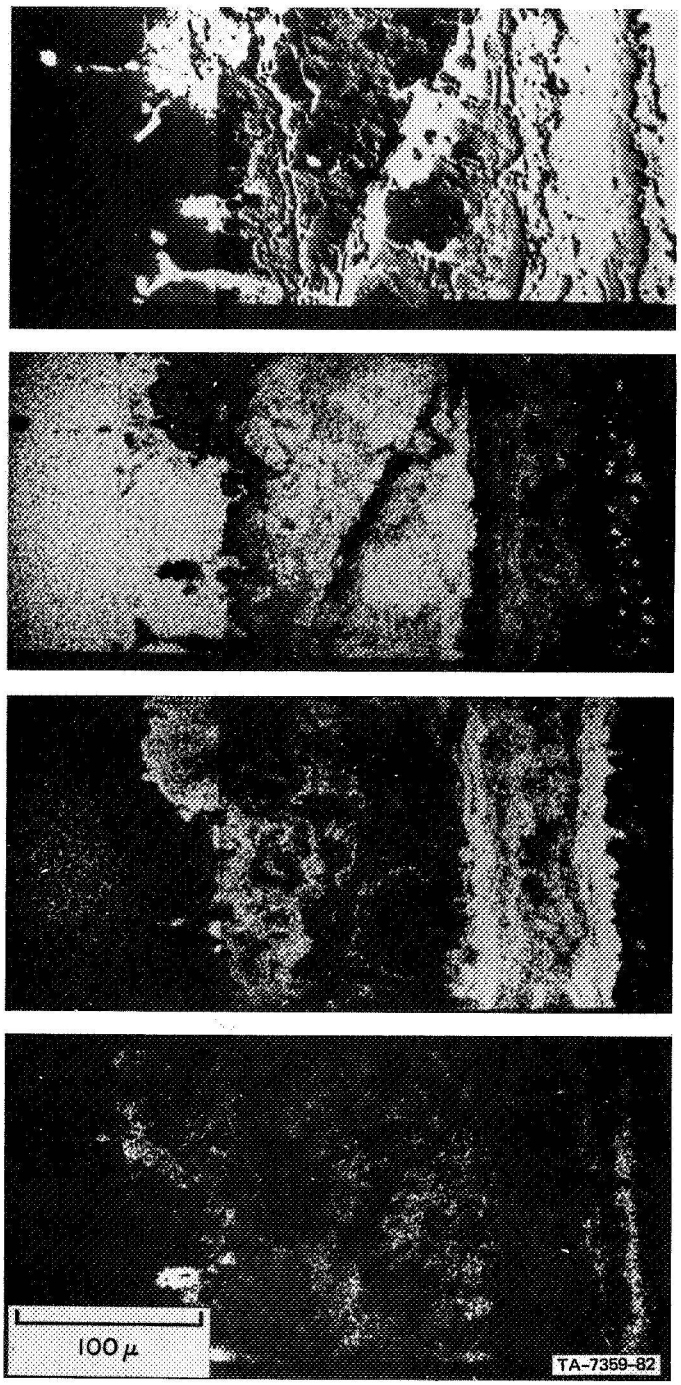

FIGURE 18 ELECTRON MICROPROBE ANALYSIS OF SCALE FORMED ON Co-20Cr-3Si OXIDIZED 2 WEEKS AT 1200°C

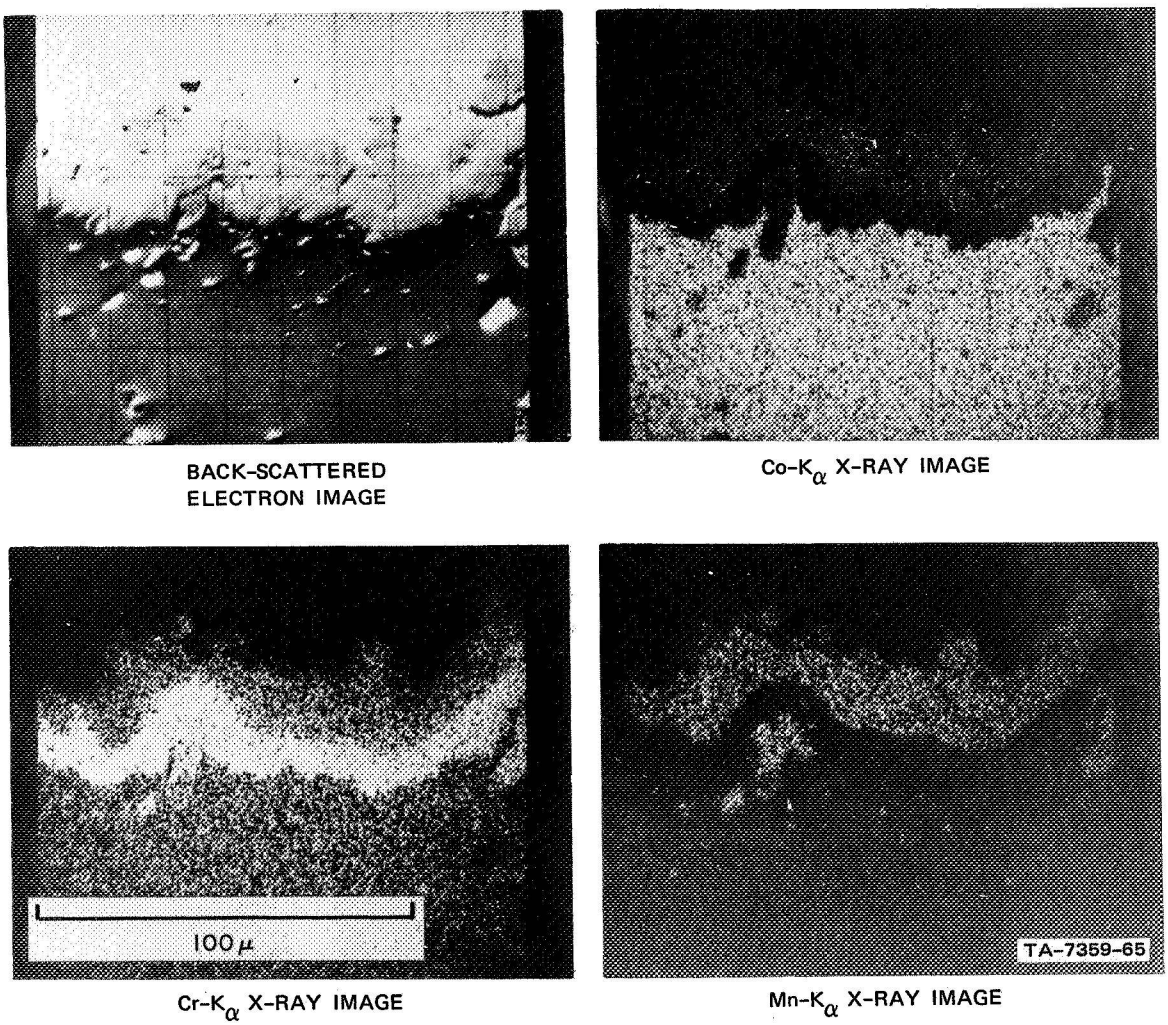

FIGURE 19 ELECTRON MICROPROBE ANALYSIS OF SCALE FORMED ON Co-20Cr-3Mn OXIDIZED 1 WEEK AT 1200°C

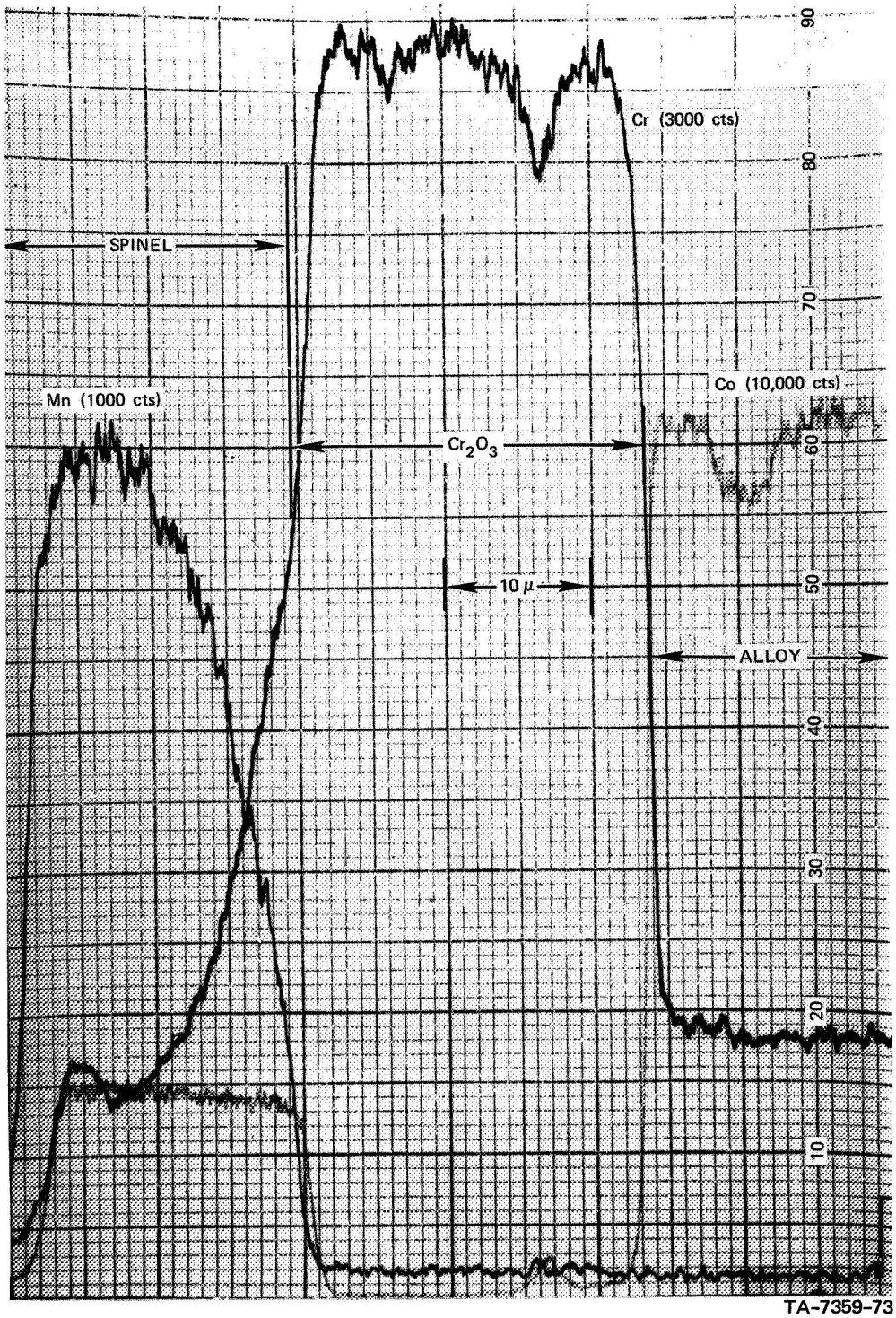

FIGURE 20 CONCENTRATION PROFILE ACROSS SCALE FORMED ON Co-20Cr-3Mn OXIDIZED 1 WEEK AT 1200°C

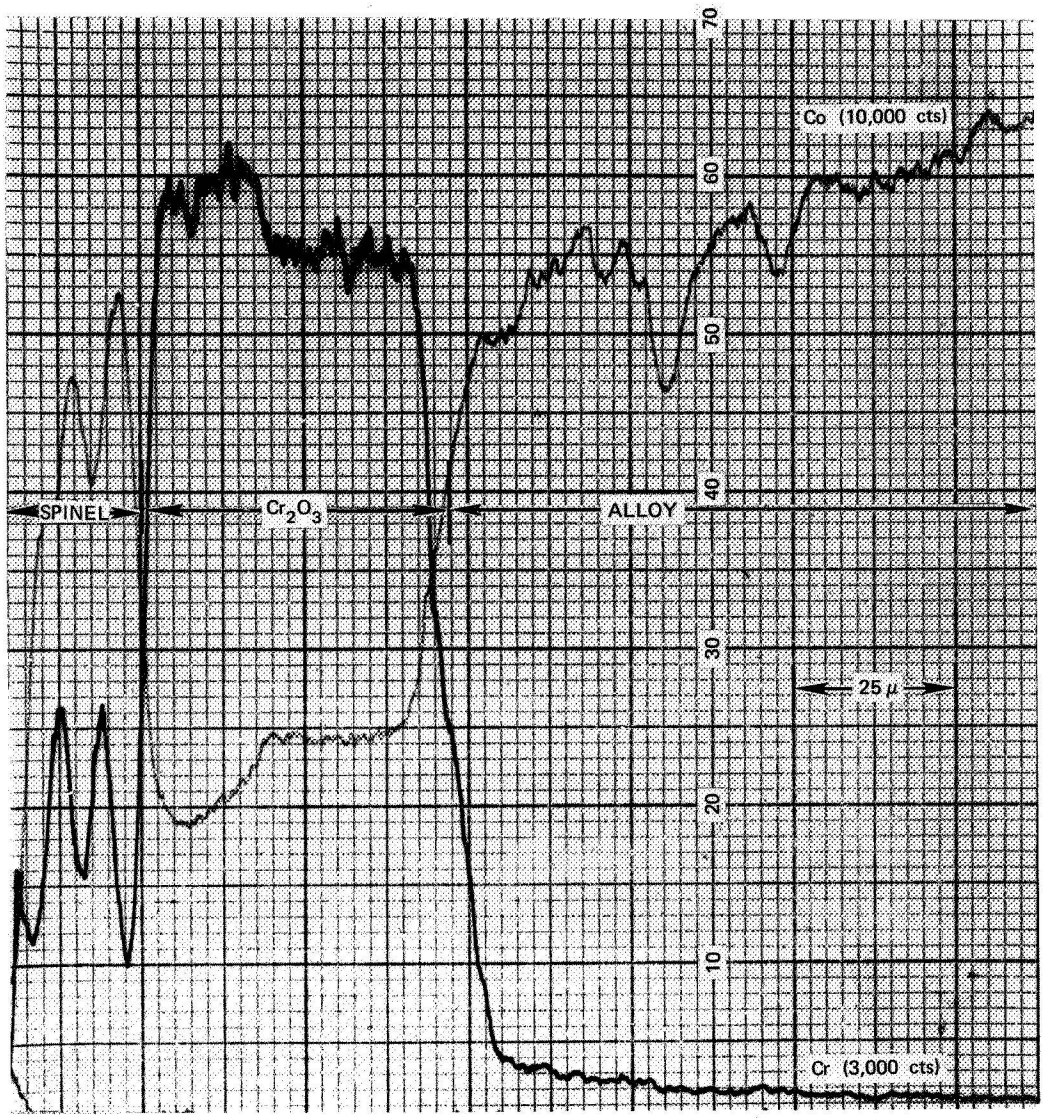

TA-7359-71

FIGURE 21 CONCENTRATION PROFILES ACROSS SCALE FORMED ON Co-20Cr OXIDIZED 2 WEEKS AT 1200°C

spinel. This particular sample was the only one that showed compositional changes in the substrate immediately below the scale. There was a slight chromium enrichment and a cobalt depletion, which is opposite the behavior that one would expect.

Nickel Alloys

Scales formed during oxidation of all the nickel-base alloys were of the compact type. No thick, duplex scales were ever observed. However, there were some notable differences, as well as some similarities, of these scales compared to those formed on the cobalt alloys. Extensive spalling occurred, and almost without exception, the outer NiO layer was lost. The micrographs almost always showed the Cr_2O_3 layers intact, whereas the spinel layer spalled although not as extensively as the NiO layer.

Scales on the base alloy, Ni-20Cr, are shown in Fig. 22. An example of a uniform Cr_2O_3 film is given in Fig. 22a (the spinel and NiO layers spalled off), and an example of a more irregular scale is shown in Fig. 22b (a small portion of the spinel is visible). The difference between these two scales is further shown in Fig. 23, which gives the electron microprobe line traverses. Figure 23a is the scale formed at 1200°C and shows only a layer of Cr_2O_3. Figure 23b is the scale formed at 1100°C and shows a sandwich of Cr_2O_3 between an outer spinel layer and a very thin, inner spinel layer.

Nickel Alloys Containing Manganese

The presence of manganese in the alloy definitely enhanced the formation of spinels in the oxide. Figure 24 clearly shows the spinels in scales formed on both the 1 and 3% manganese alloys. The main difference between the alloys containing two levels of manganese is that the higher manganese content leads to extensive spinel formation adjacent to the substrate. The undoped Ni-20Cr alloy formed only a

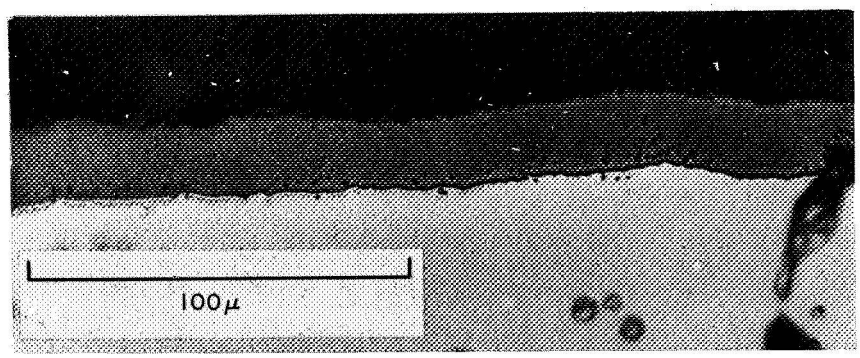

(a) UNIFORM SCALE OF Cr_2O_3 (NiO SPALLED COMPLETELY). Oxidized 1 week 1200° C.

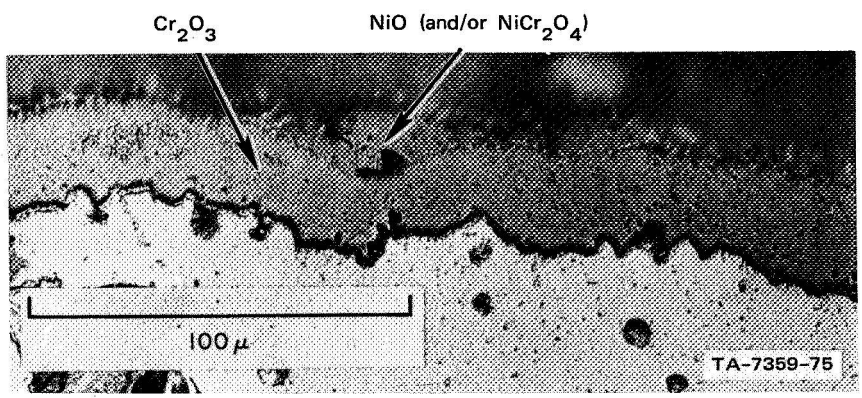

(b) IRREGULAR METAL-SCALE INTERFACE. Cr_2O_3 scale with some NiO retained on outer portion. Oxidized 3 weeks 1100° C.

FIGURE 22 SCALES FORMED ON Ni-20Cr

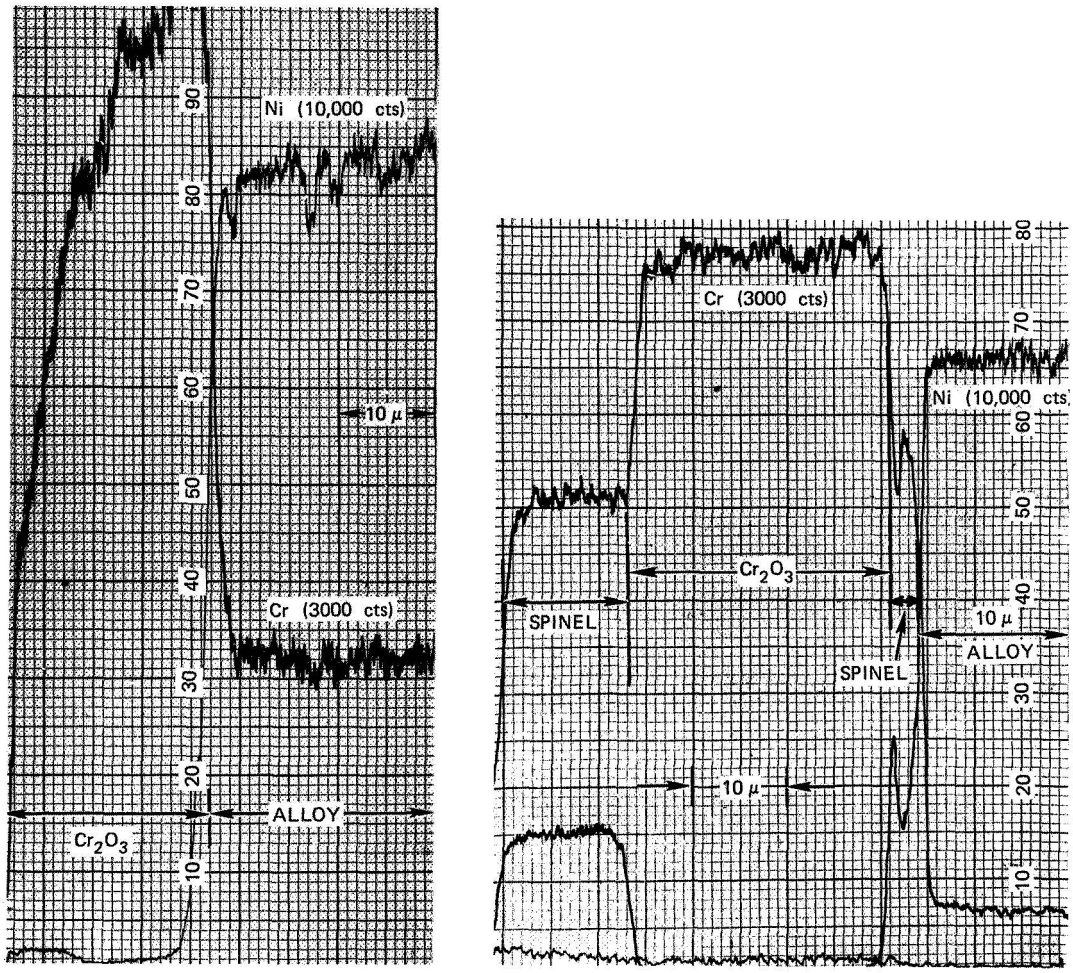

(a) OXIDIZED 2 WEEKS 1200° C

(b) OXIDIZED 3 WEEKS 1100° C

TA-7359-74

FIGURE 23 CONCENTRATION PROFILES OF SCALES FORMED ON Ni-20Cr

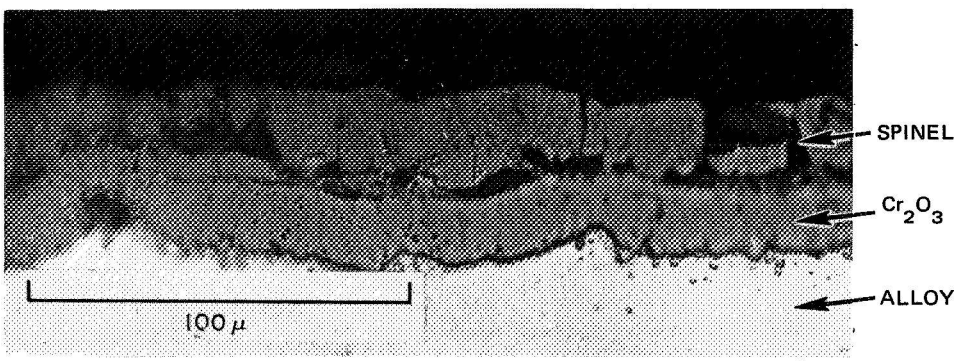

(a) SCALE FORMED ON Ni-20Cr-1Mn OXIDIZED 1 WEEK 1200° C.

(b) UNIFORM SCALE FORMED ON Ni-20Cr-3Mn OXIDIZED 3 WEEKS 1200° C.

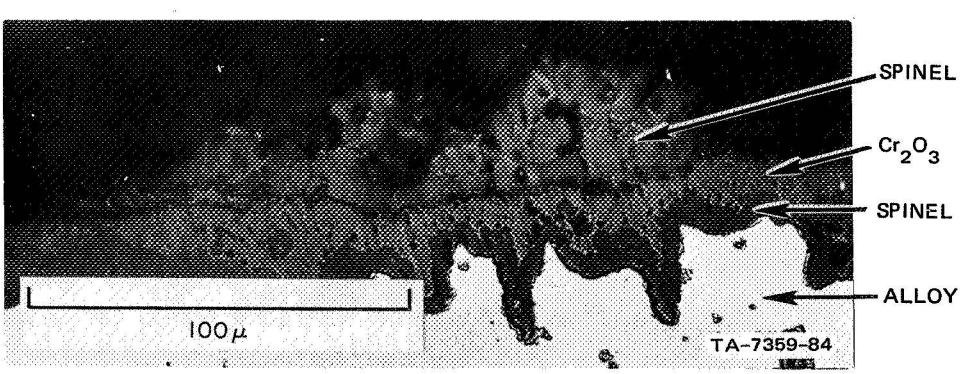

(c) IRREGULAR SCALE FORMED ON Ni-20Cr-3Mn OXIDIZED 3 WEEKS 1200°C (same sample as (b).

FIGURE 24 SCALES FORMED ON Ni-20Cr CONTAINING MANGANESE

trace of the inner spinel during three weeks oxidation at 1100°C and no spinel during two weeks of oxidation at 1200°C. On the other hand, an inner spinel layer formed on Ni-20Cr-3Mn which was as thick as the Cr_2O_3 layers in some cases (Fig. 24c). One percent manganese was not sufficient to alter the behavior of Ni-20Cr; the scales were nearly identical for alloys with and without 1% Mn.

X-ray image micrographs and concentration profiles for both manganese-containing alloys are shown in Figs. 25-28. The profile in Fig. 27a indicates that an island of spinel existed within the NiO outer layer. The thin layer of spinel that formed between the NiO and Cr_2O_3 is also apparent. A much thicker spinel layer formed adjacent to the Cr_2O_3 in the Ni-20Cr-1Mn alloy oxidized for three weeks at 1100°C. Although no NiO was detected in this particular area, there were very small remnants of NiO in other areas; most of the NiO spalled from this alloy. The variation in manganese content between the two spinels formed on Ni-20Cr-3Mn can be seen in Fig. 28. The outermost spinel contained more manganese and considerably less chromium than the inner spinel.

One other observation of interest should be noted. Under most oxidizing conditions, the Ni-20Cr-3Mn alloy formed an internal oxide phase which was shown by X-ray diffraction to be of the η-Fe_3W_3C type structure. This phase, shown in Fig. 29, was found by electron microprobe analyses to contain virtually no manganese. The probable composition is Ni_3Cr_3O. The phase was fairly massive and existed throughout the sample. It was in no way comparable to the types of oxide normally associated with internal oxidation, e.g., a layer of very fine particles of the more active component lying just below the external film.

Nickel Alloys Containing Silicon

The oxidation of these alloys was characterized by the formation of silica (alpha-cristobalite) in the scales between the alloy and a layer of Cr_2O_3 (Fig. 30). The amount of silicon in the 1% alloy was

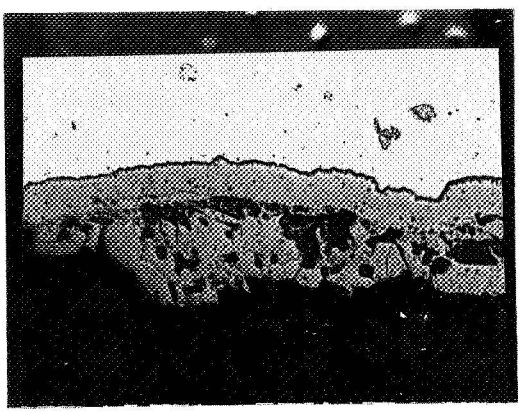

MICROGRAPH

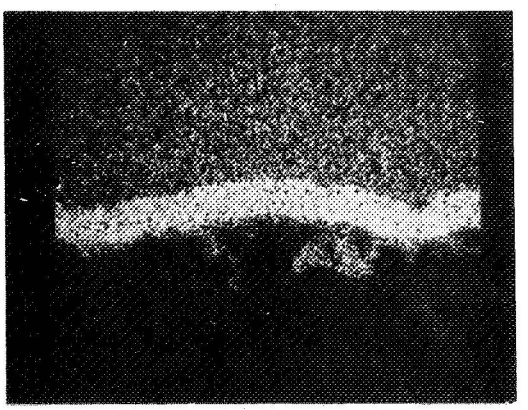

$Cr\text{-}K_{\alpha}$
X-RAY IMAGE

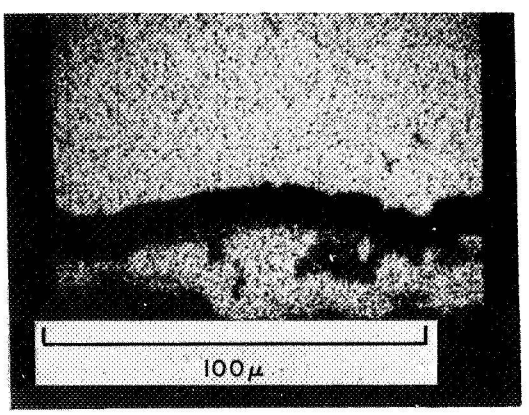

$Ni\text{-}K_{\alpha}$
X-RAY IMAGE

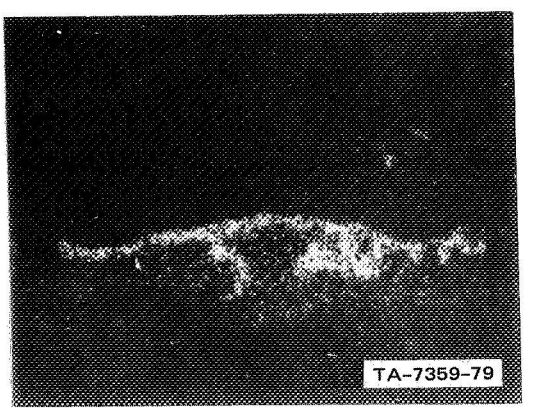

$Mn\text{-}K_{\alpha}$
X-RAY IMAGE

FIGURE 25 ELECTRON MICROPROBE ANALYSIS OF SCALE FORMED ON Ni-20Cr-1Mn OXIDIZED 2 WEEKS AT 1200°C

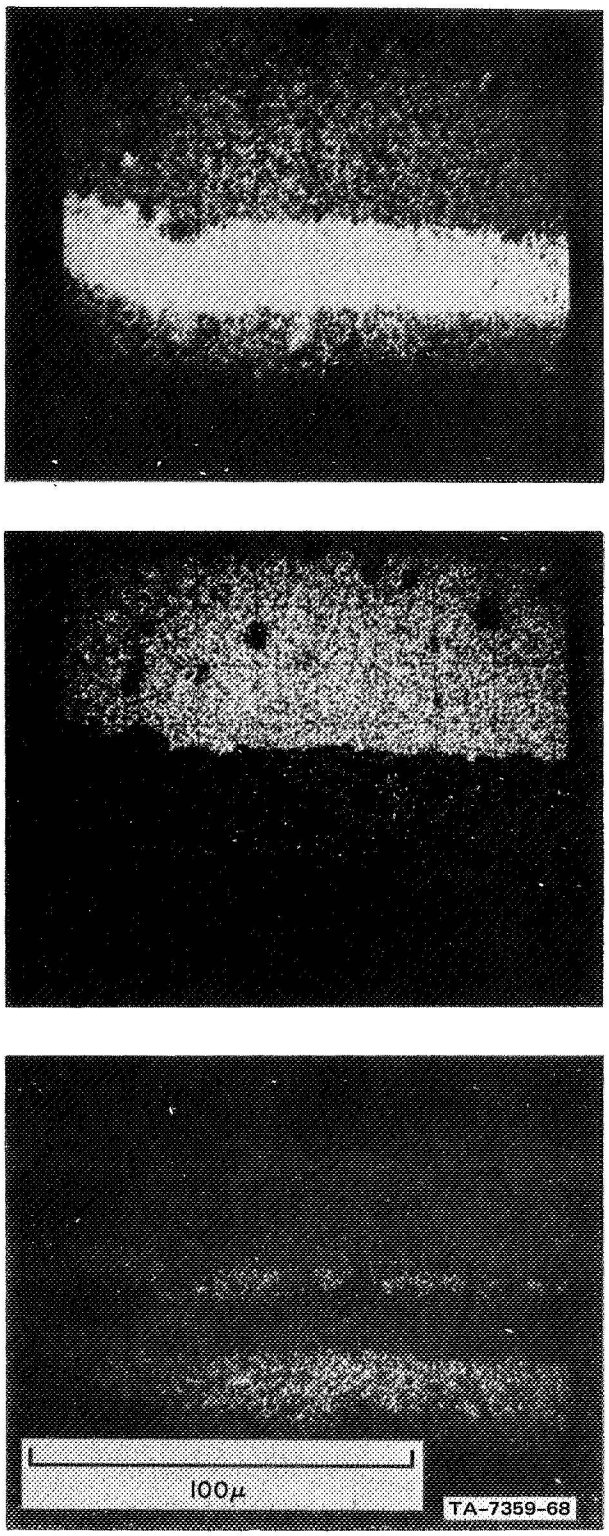

FIGURE 26 ELECTRON MICROPROBE ANALYSIS OF SCALE FORMED ON Ni-20Cr-3Mn OXIDIZED 1 WEEK AT 1200°C

FIGURE 27a CONCENTRATION PROFILES IN SCALES FORMED ON Ni-20Cr-1Mn OXIDIZED 2 WEEKS AT 1200°C

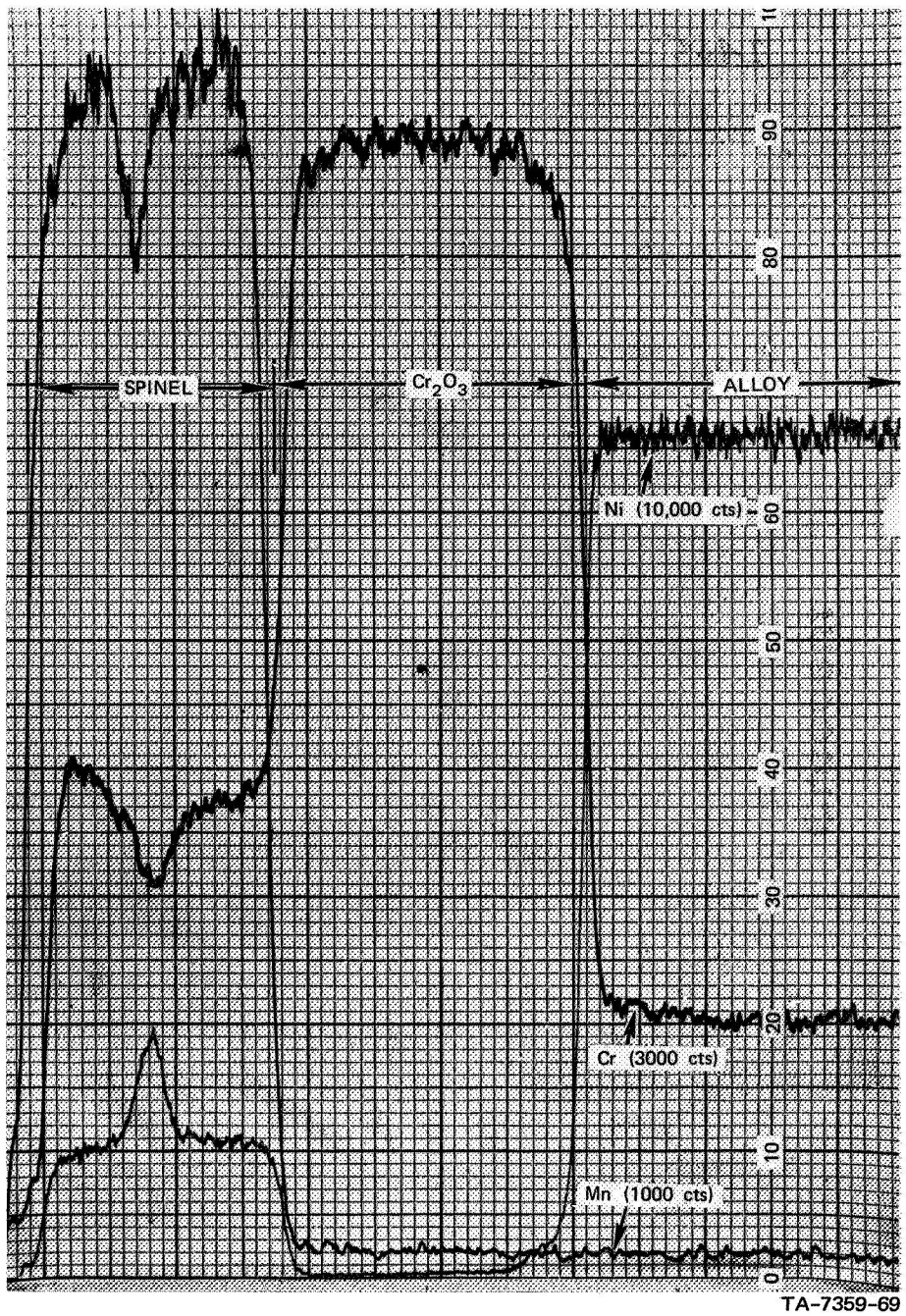

FIGURE 27b CONCENTRATION PROFILES IN SCALES FORMED ON Ni-20Cr-1Mn OXIDIZED 3 WEEKS AT 1100°C

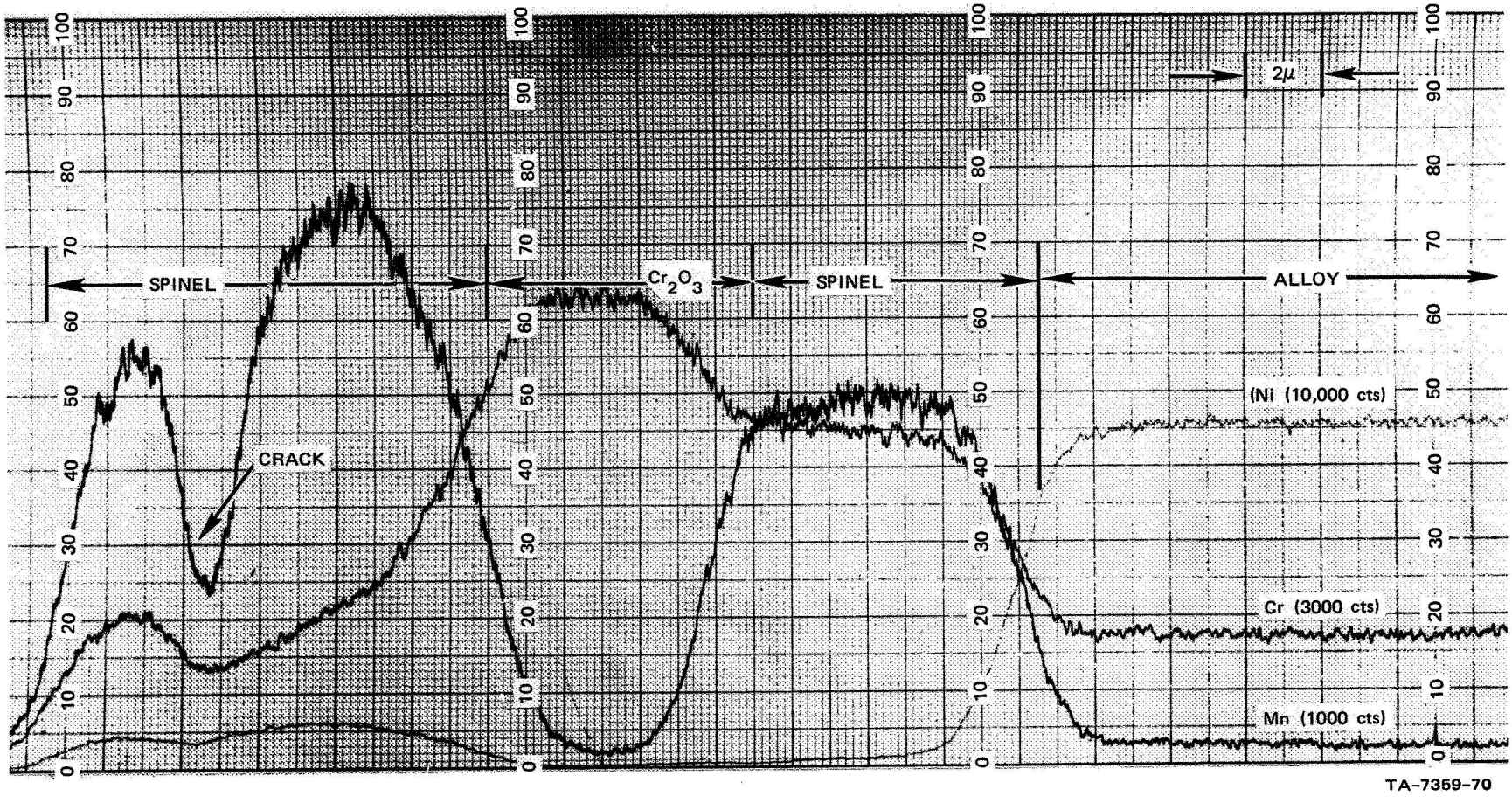

FIGURE 28 CONCENTRATION PROFILES IN SCALE FORMED ON Ni-20Cr-3Mn OXIDIZED 3 WEEKS AT 1200°C

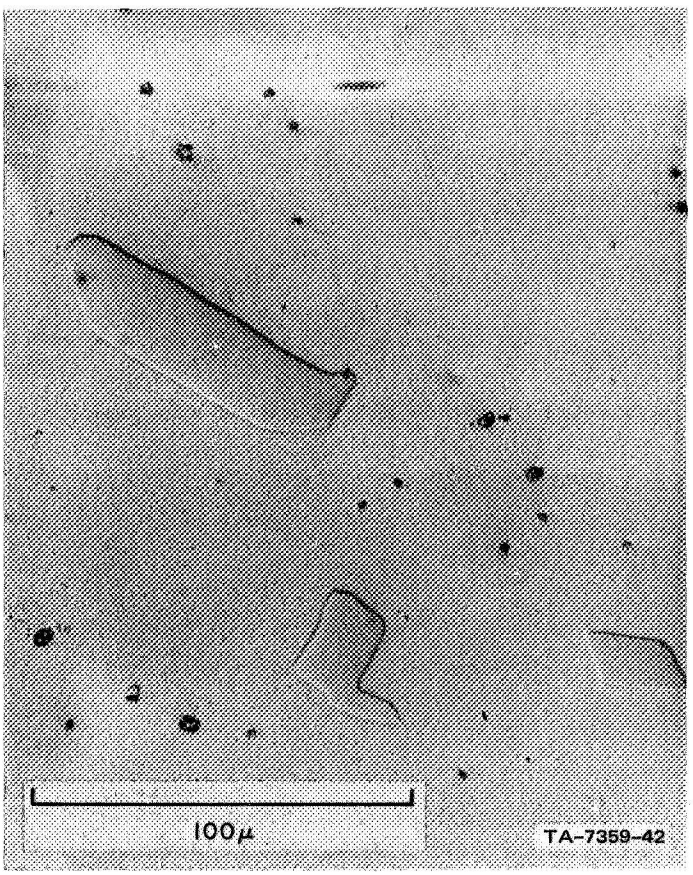

FIGURE 29 INTERNAL PHASE FORMED DURING OXIDATION OF Ni-20Cr-3Mn HAVING $E9_3$ STRUCTURE (η-Fe_3W_3C type) AND PROBABLE COMPOSITION OF Ni_3Cr_3O. No manganese was detected in this phase by microprobe analysis.

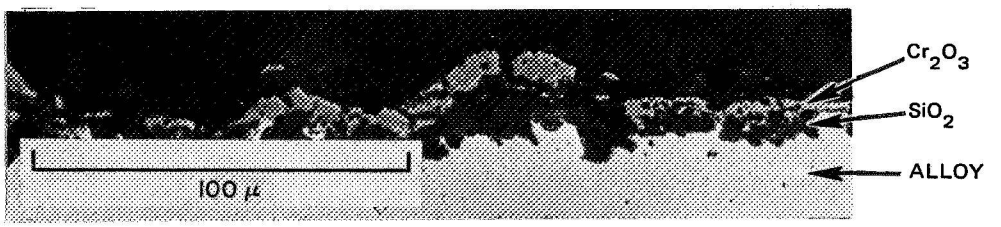

(a) Ni-20Cr-1Si OXIDIZED 2 WEEKS AT 1200° C. Nearly complete layer of SiO_2 between Cr_2O_3 and metal.

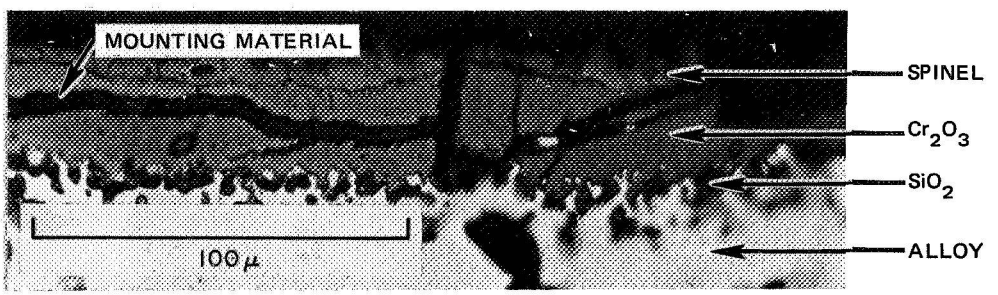

(b) Ni-20Cr-1Si OXIDIZED 1 WEEK AT 1200° C. Isolated particles of SiO_2.

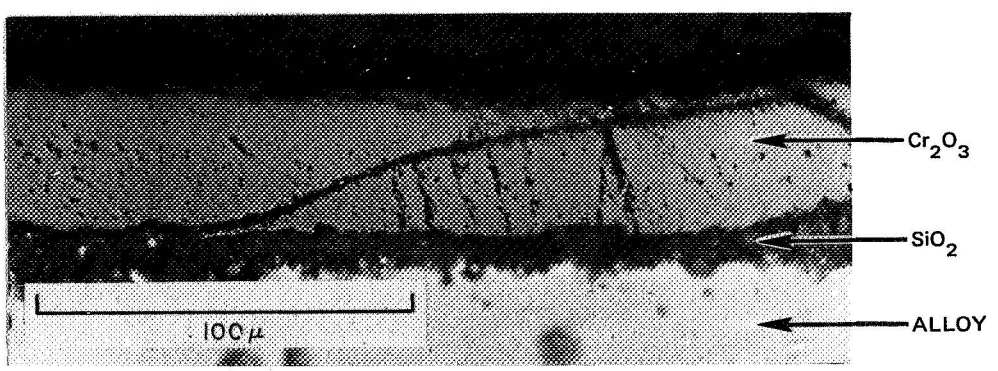

(c) Ni-20Cr-3Si OXIDIZED 1 WEEK 1200° C. Continuous film of SiO_2 between metal and Cr_2O_3 layer.

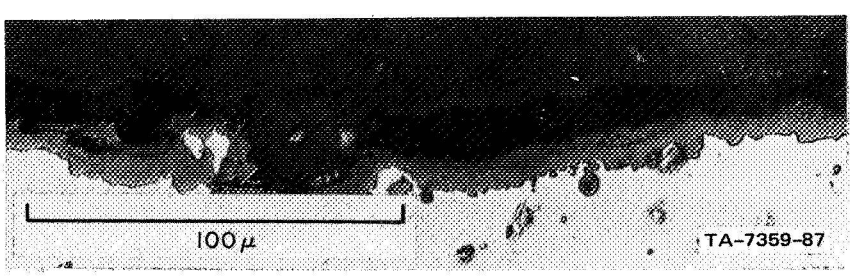

(d) Ni-20Cr-3Si OXIDIZED 2 DAYS AT 1000° C. Three phase film showing no SiO_2.

FIGURE 30 STRUCTURES OF SCALES FORMED ON Ni-20Cr CONTAINING SILICON

generally insufficient to form a continuous film of silica, whereas a continuous film of silica formed in the scales of alloys containing 3% silicon. It apparently required considerable time for the silica to form, as can be seen from the scale formed during two days oxidation at 1000°C (Fig. 30d). Although silicon is very reactive toward oxygen, the formation of SiO_2 in the scale requires diffusion of silicon in the alloy to the scale. Hence high temperatures and/or long times are required. However, the scales spalled extensively during cooling and were extremely sensitive to thermal shock.

X-ray images of the scale formed on Ni-20Cr-1Si are shown in Fig. 31. The discontinuous nature of the SiO_2 film is readily apparent. Line tranverses (Fig. 32) also point out the presence of SiO_2. A small particle of spinel existed in the Cr_2O_3 layer; the outer layer of NiO spalled during cooling.

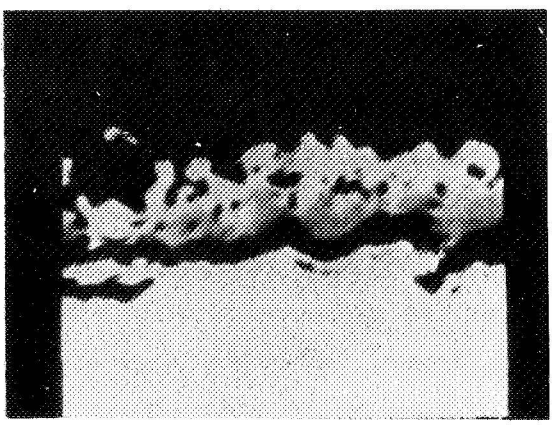

BACK-SCATTERED
ELECTRON IMAGE

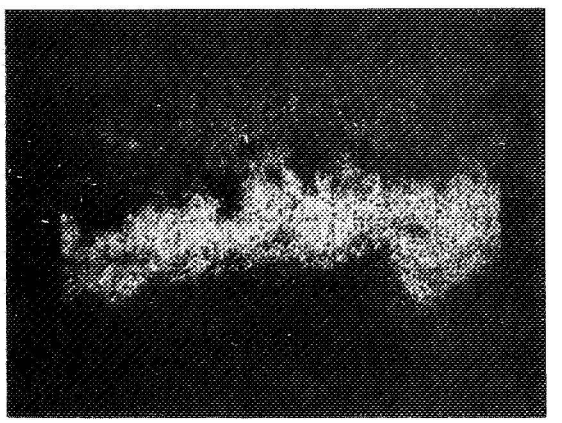

$Cr\text{-}K_{\alpha}$
X-RAY IMAGE

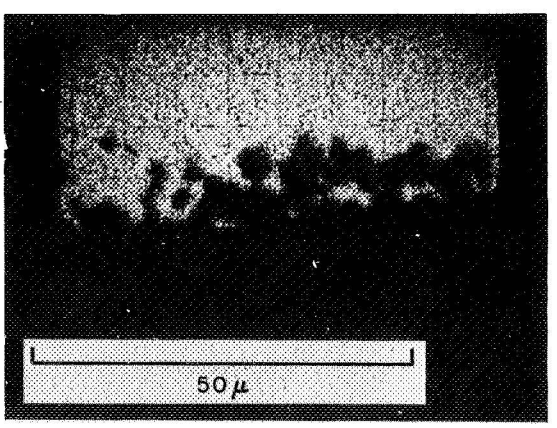

$Ni\text{-}K_{\alpha}$
X-RAY IMAGE

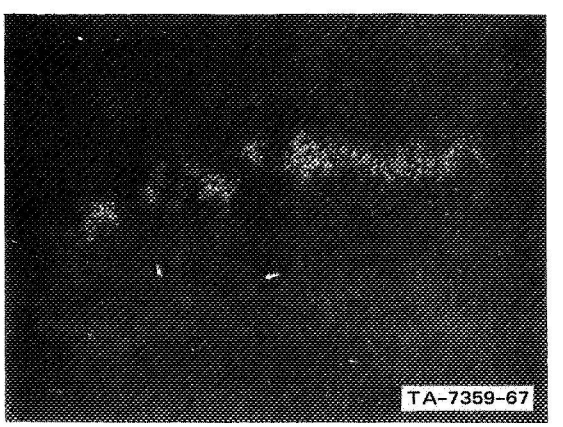

$Si\text{-}K_{\alpha}$
X-RAY IMAGE

FIGURE 31 ELECTRON MICROPROBE ANALYSIS OF SCALE FORMED ON Ni-20Cr-1Si OXIDIZED 2 WEEKS AT 1200°C

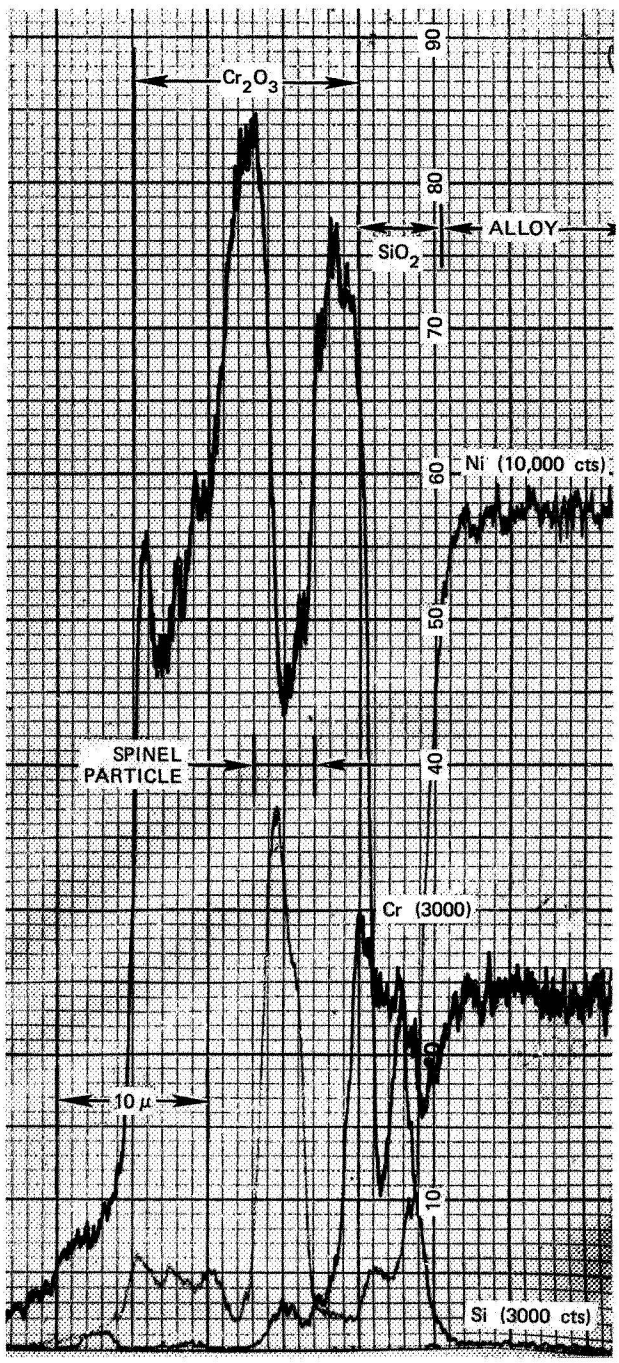

FIGURE 32 CONCENTRATION PROFILES IN SCALE FORMED ON Ni-20Cr-1Si OXIDIZED 2 WEEKS AT 1200°C

DISCUSSION

Nickel Alloys

The results of X-ray diffraction, metallography, and electron microprobe analyses can be combined to give an overall picture of the oxidation behavior of Ni-20Cr and of the effect of silicon and manganese.

In the oxidation of Ni-20Cr, the first oxide to form is NiO. This may seem surprising in view of the much higher reactivity of chromium toward oxygen than that of nickel, but the amount of nickel so overwhelms the amount of chromium that NiO forms initially. This fact has been established beyond doubt by X-ray diffraction of films formed during short oxidation periods.

NiO is not a very protective oxide compared to Cr_2O_3 (although NiO is considerably more protective than CoO on cobalt alloys), and the initial oxidation rate is fairly high. However, the formation of NiO is accompanied by an enrichment of the substrate in chromium immediately below the NiO film. The chromium is then preferentially oxidized in this zone to form a continuous film of Cr_2O_3. Twenty percent chromium is above the critical composition necessary to form a continuous layer by internal oxidation at temperatures above at least 900°C. This is not true at lower temperatures, say 600°C as can be seen in Fig. 33. At the lower temperature discrete particles of Cr_2O_3 form and eventually coalesce into a continuous film. However, the bulk of this work was performed at higher temperatures, at which the continuous film was the rule.

Once the Cr_2O_3 film had formed, it thickened slowly with increasing time. The solubility of nickel in Cr_2O_3 is very small, and very little diffusion of nickel occurred through the Cr_2O_3 layer. Thus, the further growth of NiO was effectively halted, and oxidation proceeded mainly by additional Cr_2O_3 formation.

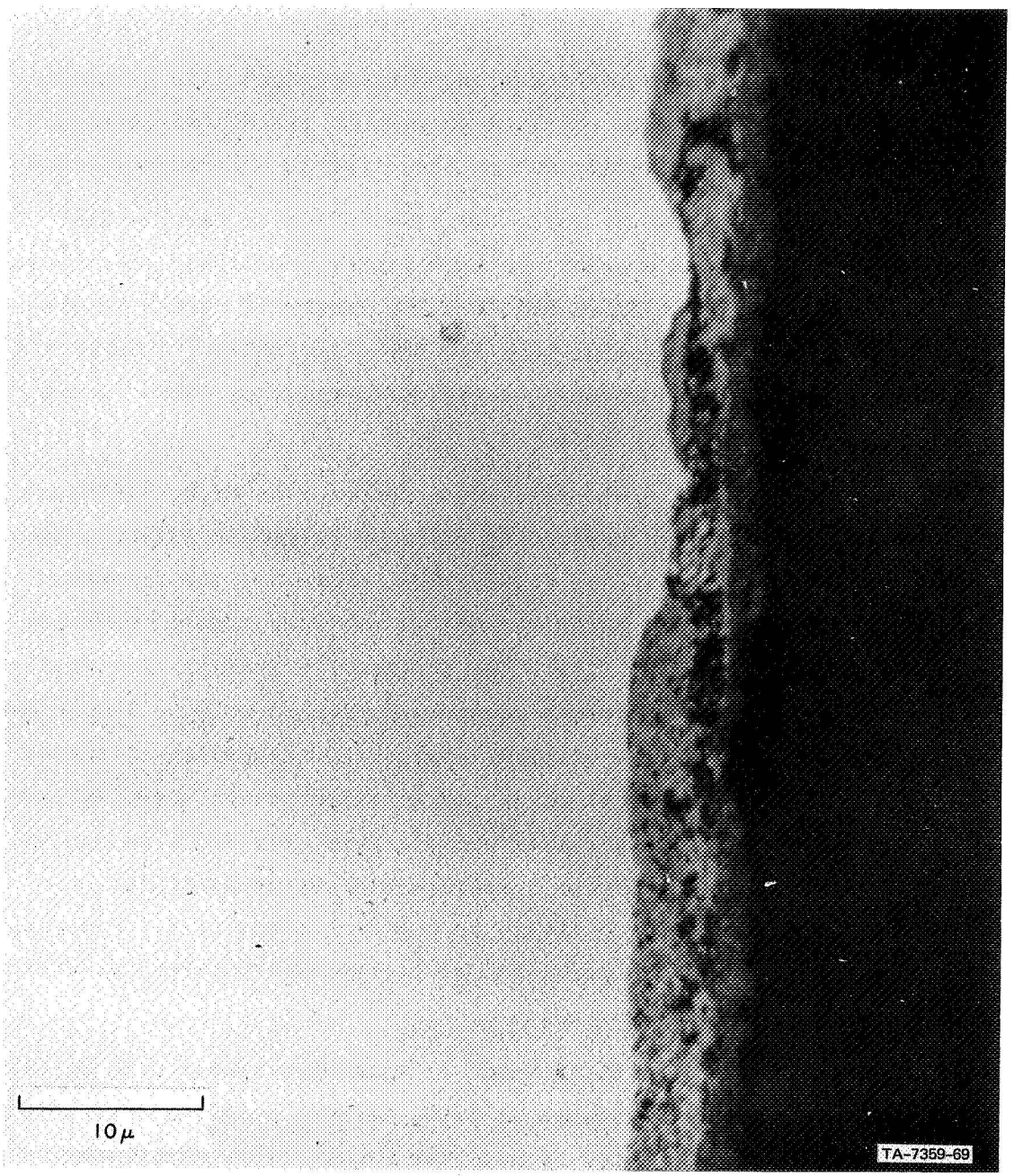

FIGURE 33 DISCRETE PARTICLES OF Cr_2O_3 FORMED BY INTERNAL OXIDATION BENEATH EXTERNAL SCALE ON Ni-20Cr OXIDIZED 40,000 MINUTES AT 600°C

However, a composite layer of NiO adjacent to Cr_2O_3 is thermodynamically unstable at high temperatures, and the following reaction occurs:

$$NiO + Cr_2O_3 = NiCr_2O_4$$

The product is a spinel that forms at the expense of the NiO. Additional Cr_2O_3 forms at the oxide-metal interface. Eventually all the NiO is consumed, if the oxidation is carried out for sufficiently long times. The scale structure will ultimately be an outer layer of spinel and an inner layer of Cr_2O_3. The spinel layer should reach some limiting thickness related to the amount of NiO that initially formed and the densities of the compounds.

The formation of spinel is contrary to what Wood et al. have reported.[5,6] Their electron microprobe analyses showed no evidence of spinel, and they concluded that the protectiveness of the film on Ni-Cr alloys was definitely associated with the presence of Cr_2O_3 and not with the presence of a spinel. Although Wood et al. did not observe spinel, they do acknowledge that its formation is thermodynamically possible. There was no further discussion of the spinel formation in their proposed oxidation mechanism.

Spinel formation was not limited to the outer part of the scale on top of the Cr_2O_3 layer. A trace of spinel was also observed in Ni-20Cr at the scale-alloy interface (Fig. 23b). This observation also contradicts Wood's statement, "The chromium concentration at the alloy-oxide interface is never reduced sufficiently for chemical transformation of the Cr_2O_3 to $NiCr_2O_4$ by the underlying alloy."* Spinel formation was not too prevalent at the oxide-metal interface in this study, but it did occur, and in particular was very extensive in the alloys containing 3% manganese. Wood's statement was based on the thermodynamic calculations of Birks and Ricker,[7] who calculated that

*Wood's observations were for oxidation times generally less than 100 hours.

The chromium value must fall to 1.4×10^{-4} % before spinel formation could occur. As will be shown subsequently, the spinel does play an important role in the oxidation of Ni-Cr alloys, and the results of this study do not confirm their conclusion that the protectiveness stems solely from Cr_2O_3.

The relatively thick spinel layers at the exterior scale result from the finite thickness of the NiO layer from which the spinel forms. Armijo[8] showed that the rate-controlling step in spinel formation from a couple of NiO and Cr_2O_3 was dissolution of chromium in NiO. Chromium diffusion is of the same order of magnitude as nickel diffusion in NiO. If the NiO layer is large, chromium diffuses further away from the interface, and no appreciable buildup of chromium occurs. Spinel cannot form until a critical value of chromium has been established in the NiO at the interface. This behavior is analogous to the oxidation behavior of the Group IV-A elements that exhibit extremely high oxygen solubilities. No external oxide layer forms until the oxygen concentration in the substrate reaches the critical value. The time to establish this value is primarily a function of the oxygen diffusivity in the metal.[9]

The Effect of Mn. The addition of manganese to the alloy has little effect at the 1% level, but at the 3% level a considerable difference in the scale structure is noted. Manganese is a strong spinel former, and its presence results in the formation of a dense, continuous spinel layer between the metal and the Cr_2O_3. It is also interesting to note that the oxidation rate at 1000°C and 1100°C is lower for the Ni-20Cr-3Mn alloy than for either Ni-20Cr or Ni-20Cr-1Mn. All three of these alloys have Cr_2O_3 layers in the scale that are continuous. However, the alloy oxidizing the slowest, Ni-20Cr-3Mn, also has a continuous spinel layer between the metal and the Cr_2O_3 that was essentially a $MnCr_2O_4$ spinel with very little nickel. The diffusivities of the cations in this structure have not been reported, but on the basis of the oxidation behavior of alloys exhibiting the $MnCr_2O_4$ layer, the diffusion rates would be expected to be low.

The rates of solid-state spinel formation of couples consisting of Cr_2O_3 and NiO doped with 1 Mol % MnO were about the same as those for Cr_2O_3 and pure NiO.[8] Manganese has about the same reactivity toward oxygen as does nickel, and MnO is isomorphous with NiO; therefore, the NiO that forms initially on the alloys containing manganese will also contain MnO. The spinel that subsequently forms between the "doped" NiO and Cr_2O_3 will contain manganese also, as is shown by the microprobe traverses. The spinel that forms at the oxide-metal interface does so by reaction of Cr_2O_3 with an alloy substrate that is highly enriched in manganese. This spinel appears to form more slowly than the outer spinel and its presence will reduce the oxidation rate. The effect is not noted initially because the outer two layers form first. The inner spinel is tenaciously bound to the metal; the outer spinel spalls readily. The Cr_2O_3 layer is also intimately bound to the inner spinel, and even though the outer spinel spalls, oxidation resistance of both the inner layers remains.

The question of whether the spinel really is protective may be readily resolved by comparing the values of the parabolic rate constants for the oxidation of pure chromium (which involves outward cation diffusion in Cr_2O_3) and that for the formation of $NiCr_2O_4$.

The parabolic rate constant for the formation of spinels is given by the expression[10-12]

$$k_p = \frac{4}{3n_A} \tilde{V} \tilde{C}_A z_A D_A \left[1 - \exp(n_A \Delta G^0/RT)\right]$$

where n_A is the dimensionless factor that is the characteristic coefficient of the defect equilibria controlling the diffusion mechanism, $\tilde{V}$ is volume of spinel formed per equivalent of A^{2+}, z_A is the absolute charge of cation A, C_A is the average concentration of A^{2+} in the spinel layer in equivalents per unit volume, D_A is the diffusion coefficient of A^{2+} in the spinel in equilibrium with AO, and ΔG^0 is the free energy of formation of the spinel from its pure component oxides. The mechanism

of spinel formation postulated by Wagner[10] involves countercurrent cation diffusion in the spinel. The reactions are shown in Fig. 34. The sequence includes the respective dissociation of the component oxides, simultaneous countercurrent diffusion of $3A^{2+}$ and $2B^{3+}$ ions across the spinel leaving excess anions in the starting oxides, and reaction of the $2B^{3+}$ ions with the excess anions and AO to form AB_2O_4 and reaction of the $3A^{2+}$ ions with excess oxygen anions and B_2O_3 to form $3AB_2O_4$.

A comparison of the experimentally determined k_p for solid-state spinel growth with the parabolic rate constant for the oxidation of pure chromium (which involves outward cation diffusion in Cr_2O_3) is shown as a function of temperature in Fig. 35, along with reported diffusivities in the spinel. The difference between the two k_p's is about a factor of 1000, the spinel formation being by far the slower process.

There is probably a slight difference in values of k_p for spinel formation by reaction of Cr_2O_3 and for spinel formation by the reaction

$$Cr_2O_3 + Ni{+}O^{-2} = NiCr_2O_4$$

Birks and Richert[7] state that the free energy for this reaction is negative just within the metal-inner oxide zone. They also give the reaction

$$4Cr_2O_3 + 3Ni = 3NiCr_2O_4 + 2\ Cr$$

for which the free energy change at 1000°C is + 84,000 cal. Although this reaction has a positive free energy change, the reaction could go to the right if the chromium content were low enough at the scale-metal interface. There was no evidence for a low value of chromium from the electron probe traverses; however, the beam size of approximately 2 microns could have overlapped such a zone and precluded its identification. The important fact is that the spinel was found at the scale-metal interface, and even if the thermodynamics are not particularly favorable, the spinel forms.

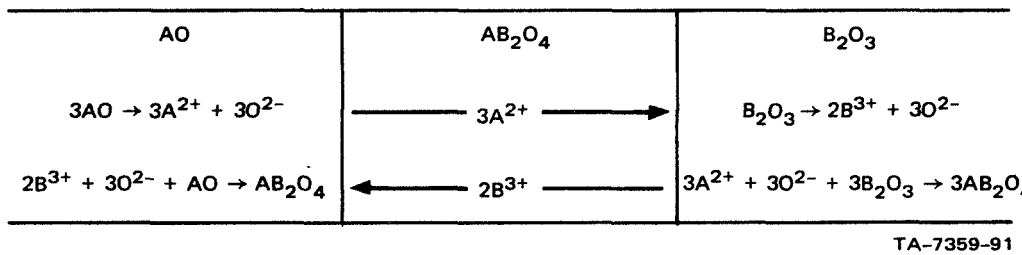

FIGURE 34 SPINEL GROWTH MECHANISM
(Wagner-Schmalzried Model)

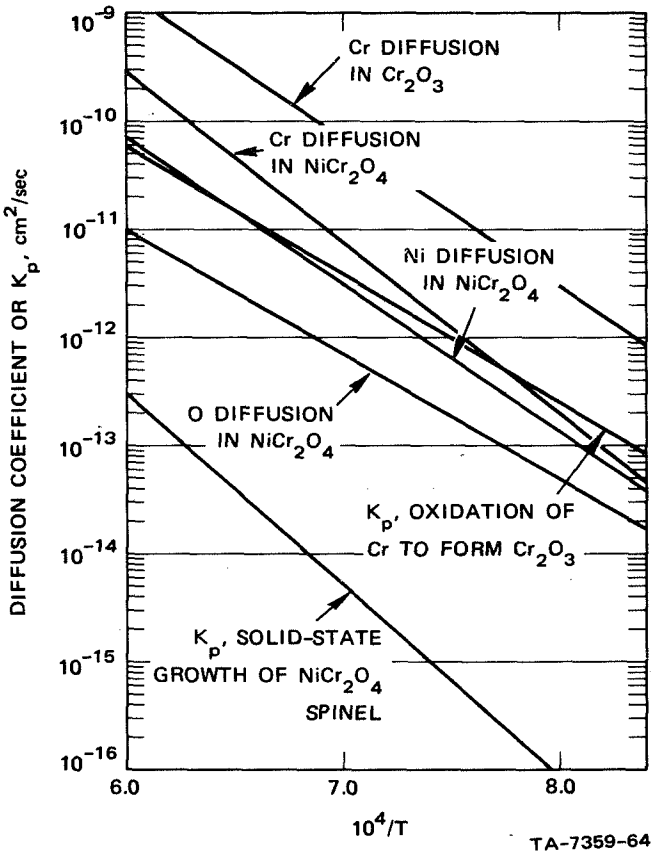

FIGURE 35 COMPARISON OF VARIOUS PROCESSES RELATING TO OXIDATION OF Ni-20Cr

It thus can be concluded that the presence of manganese is generally beneficial when it promotes the formation of an inner spinel layer. The outer spinel layer is generally lost by spalling and offers little protection, but the inner spinel is tightly adherent, and the slow rate of ion transport across this layer increases the oxidation resistance.

The above conclusion is in contradiction to the statment by Evans et al.[13] that spinels are not responsible for low scaling rates in Ni-Cr alloys. They also conclude that the spinel existing in the scales of oxidized Ni-Mn alloys was not the protective layer. However, they do not distinguish between an outer spinel scale that readily spalls and an inner spinel layer that does not spall and that is responsible for low scaling rates.

The Effect of Silicon. Additions of silicon reduced the rate of oxidation at all temperatures, although the films formed were very susceptible to spalling upon cooling from the oxidation temperature. Metallographic examination and microprobe traverses definitely established that a layer of SiO_2 (alpha cristobalite form) existed at the oxide-metal interface. However, as in the case of plain Ni-20Cr or those alloys containing manganese, NiO formed initially, then Cr_2O_3 formed beneath the NiO. The NiO and Cr_2O_3 reacted to form an outer spinel layer. The big difference between alloys containing silicon and those containing manganese was that those containing silicon did not form an inner spinel layer but rather formed SiO_2.

The solubility of most elements in SiO_2 is virtually nil, and consequently there is very little driving force (low chemical) potential gradient) for diffusion of such elements as chromium or nickel through SiO_2.[14] It is not unreasonable to expect that those alloys that are capable of forming a continuous, defect-free film of SiO_2 should exhibit a very low oxidation rate. The only reason that the rates are not lower than observed is that the SiO_2 layer is not continuous. The alloy containing 3% silicon had a more nearly continuous film than the

alloy containing 1% silicon. The former also oxidized more slowly than the latter. It thus appears that oxidation resistance can be improved by silicon additions, notwithstanding the fact that the outer films spall extensively.

Cobalt Alloys

The oxidation of Co-20Cr is analogous to that of Ni-20Cr with some small exceptions. The first oxide to form is CoO, which forms at a rate about 100 times faster than the NiO formed on Ni-20Cr. As in the case of nickel alloys, the substrate becomes enriched in chromium, and a layer of Cr_2O_3 eventually forms. The main difference between the cobalt alloys and the nickel alloys is that the reaction between CoO and Cr_2O_3 to form cobalt-chromium spinel is nearly 10,000 times faster than the growth rate of $NiCr_2O_4$. The much faster reaction rate for the cobalt spinel means that more spinel will form per unit time and that the Cr_2O_3 will be used up faster than new Cr_2O_3 grows. This statement can be verified by Fig. 36, which compares the growth rates of the two processes. The more rapid growth rate of spinel compared to Cr_2O_3 means that Cr_2O_3 is more protective than $CoCr_2O_4$. This behavior is opposite that observed in the nickel alloys. The thick scales such as those shown in Fig. 12-b and 16 consist of an outer CoO layer and an inner layer of spinel interspersed with CoO. There appears to be no Cr_2O_3.

Certain parts of the scales formed on Co-Cr alloys, as indicated previously, are much thinner than other parts on the same sample. The above discussion pertains only to the thick portions. Fig. 20, for example, clearly shows the presence of a continuous layer of Cr_2O_3. The explanation for these differences is not clear. If heterogeneities in composition were considered, there should be a certain randomness to the location of thick and thin scales. However, the thick scales were always confined to the ends of the samples, whereas the thin portions were associated with the flat surfaces. This observation leads one to suggest that geometric considerations apply. One ramification of the

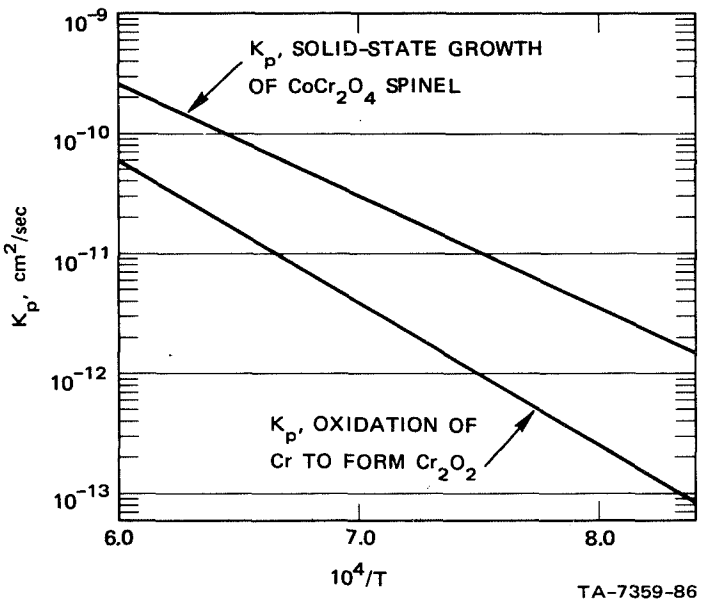

FIGURE 36 COMPARISON OF GROWTH RATES OF Cr_2O_3 AND $CoCr_2O_4$

sample geometry is the restraints offered by edges and corners to plastic deformation of the oxides. This phenomenon has been observed extensively in the formation of sulphides on copper, nickel, and iron.[15,16,17] The same kind of "dog bone" structure occurred as was observed in the oxidation of the cobalt-chromium alloys. Basically, the mechanism is simply that the epitaxial mismatch stresses are more than sufficient to plastically deform the scale over the flat parts, and consequently the extremely large number of cation vacancies cannot coalesce to form voids. The plastic deformation of the oxide closes the voids as soon as they form. The source of the vacancies is at the oxide-gas interface. One cation vacancy is created for each anion taken into the scale. The cation vacancies subsequently move inward countercurrently to the outward flux of cations.

Restraint of the oxide at the edges prevents the closure of the pores. The thick, porous scale is the result of increased diffusion of cobalt ions by means of surface diffusion on the inside surface of the pores.

The Effect of Manganese. The compact scales formed on manganese-containing alloys consisted of an inner and outer spinel with a layer of Cr_2O_3 between. The structure of the scales was analogous to that on the nickel alloys with manganese. The inner spinel was richer in manganese than the outer spinel. The inner spinel was not always present in the scales of Co-20Cr-3Mn (Fig. 20). On the other hand, an inner spinel, $CoCr_2O_4$, sometimes formed on plain Co-20Cr alloys, and in other cases only the outer spinel was observed on this alloy.

The influence of manganese on the kinetics of oxidation of Co-20Cr is not too clear because of the extensive spalling that occurred during testing and the heterogeneous nature of the scales formed. However, if one could disregard these problems, it would appear on the basis of Armijo's work[8] that, although the presence of manganese decreases the solid-state growth rate of $CoCr_2O_4$, its rate of growth still exceeds that of Cr_2O_3. Thus, the Cr_2O_3 is still more protective than

a slightly doped cobalt-manganese chromium spinel, and if the doped spinel forms faster than the Cr_2O_3, the protective layer of Cr_2O_3 is used up faster than it forms. The overall effect of manganese is nearly nil. It is conceivable, however, that higher manganese contents than those used in this program might prove beneficial if a manganese-chromite could form in preference to the doped cobalt chromite.

The Effect of Silicon. The presence of silicon in Co-20Cr alloys resulted in the formation of Co_2SiO_4 in the scales as was shown in several of the micrographs. Furthermore, under certain conditions internal oxidation within the alloy also occurred (Fig. 15b). Generally, the scales on these alloys were highly irregular (Fig. 15a), and spalling was extensive.

The addition of silicon decreases the oxidation rate of Co-20Cr at 1200°C. The effect at lower temperatures cannot be determined because of excessive film spalling. Alloys containing 3% silicon did not exhibit the heterogeneity of the scales that the other alloys did, although there was still a tendency to form "dogbone" structures.

The apparent decrease in oxidation rate by the addition of silicon is puzzling in view of the observed effect of silicon on the rate of formation of $CoCr_2O_4$.[8] A one to two order of magnitude increase in growth rate occurred when the CoO (in $CoO-Cr_2O_3$ couples) was doped with 1.5 mol % SiO_2. The measurements were made at fairly high temperatures, and it was noted from the appearance of the structures that "the wetting by the matrix phase suggests that the spinel and orthosilicate crystals grew in either a liquid or semiliquid phase." If this were the case, the considerably higher growth rate of the spinel could be attributed to diffusion in a liquid or "mushy" matrix which would be much more rapid than solid-state diffusion. However, the structure of scales formed on cobalt alloys containing silicon were dissimilar from the structure of the silica-doped CoO/Cr_2O_3 couple reaction zone. This indicates that there was no liquid phase present during oxidation. The

higher temperatures employed in the spinel work [8] and the fact that a eutectic exists at 1370°C in the $CoO-SiO_2$ system (the eutectic temperature for the ternary system $CoO-SiO_2-Cr_2O_3$ would probably be even lower) account for the much more rapid formation of spinel and silicate in the diffusion couples than in the oxide scales.

The slower oxidation rate of Co-20Cr containing silicon compared to that of either plain Co-20Cr or Co-20Cr with manganese is most likely due to the presence of the thin layer of Cr_2O_3 shown in Fig. 15. This scale is protective at the oxidation temperature, but the looseness of the undulating layer gives rise to excessive spalling.

REFERENCES

1. J. W. Hickman and E. A. Gulbransen, "An Electron Diffraction Study of Oxide Films Formed on Nickel-Chromium Alloys,"Trans. AIME, 180, 519 (1949).

2. M. Sygiyama and T. Nakayama, "Effect of Si on High Temperature Oxide Films in Heat-Resisting Alloys," Japan Inst. Metals J., 24 541 (1960).

3. E. A. Gulbransen and W. R. McMillan, "Oxide Films on Nickel-Chromium Alloys," Ind. Eng. Chem. 45, 1734-44 (1953).

4. E. A. Gulbransen and K. F. Andrew, "Oxide Studies on Nickel-Chromium and Nickel-Chromium-Aluminum Heater Alloys," J. Electrochem. Soc., 106, 941, (1959).

5. G. C. Wood and T. Hodgkiess, "Characteristic Scales on Pure Nickel-Chromium Alloys at 800-1200°C," J. Electrochem. Soc., 113, 319, (1966).

6. G. C. Wood, T. Hodgkiess, and D. P. Whittle, "A comparison of the Scaling Behavior of Pure Iron-Chromium and Nickel Chromium Alloys in Oxygen," Corr. Sci., 6, 129 (1966).

7. N. Birks and H. Rickert, "The Oxidation Mechanism of Some Nickel-Chromium Alloys," J. Inst. Metals, 91, 308 (1962-63).

8. J. S. Armijo, "Mechanisms and Kinetics of Nickel Chromite and Cobalt Chromite Spinel Formation," NASA-Cr-72537 (1969).

9. P. Kofstad, High Temperature Oxidation of Metals, J. Wiley and Sons, New York, 166 (1966).

10. C. Wagner, "On the Mechanism of Formation of Ionically Bonded Higher Order (Double Salts, Spinels, Silicates)," Z. Phys. Chem., 34, 309 (1936).

11. H. Schmalzried, "Reaction Mechanisms of Spinel Formation in the Solid State," Z. Phys. Chem. (N.F.), 33, 111 (1962).

12. H. Schmalzried, "Solid State Reactions," Ber. Deut. Keram. Ges., 42, 11 (1965).

13. E. B. Evans, C. A. Phalnikar, and W. M. Baldwin, Jr., "High Temperature Scaling of Nickel-Manganese Alloys," J. Electrochem. Soc., 103, 367 (1956).

14. I. S. Gil'dengorn, and I. L. Rogel'berg, "Effect of Silicon Additions on the Oxidation of the Alloys of Nickel with 10% Cr," 18, 935 (1964).

15. A. Bruckmann, S. Mrowec, and T. Werber, "Reaction Diffusion Mechanism in the System Copper-Sulpher," Fiz. Metal Metalloved., 15 (1963), 1003 p. 35.

16. L. Czerski, S. Mrowec, and T. Werber, "Kinetics and Mechanism of Nickel-Sulfur Reaction," J. Electrochem. Soc., 109 273 (1962).

17. R. A. Meussner and C. E. Birchenall, "The Growth of Ferrous Sulfide on Iron," Corrosion, 13, 677t (1957).

DISTRIBUTION LIST

CONTRACT NAS 3-11165 - STANFORD RESEARCH INSTITUTE

REPORT NO. NASA CR-72607

National Aeronautics and Space Administration
Washington, D. C. 20546

Attention:	N. F. Rekos (RAP)	1
	G. C. Deutsch (RRM)	1
	R. H. Raring (RRM)	1

Lewis Research Center
National Aeronautics and Space Administration
21000 Brookpark Road
Cleveland, Ohio 44135

Attention:	G. M. Ault, MS 105-1	1
	Technology Utilization Office, MS 3-19	1
	R. W. Hall, MS 105-1	1
	Library, MS 60-3	2
	Report Control Office, MS 5-5	1
	S. J. Grisaffe, MS 49-1	1
	Dr. H. B. Probst, MS 49-1	1
	N. T. Saunders, MS 105-1	1
	F. H. Harf, MS 106-1	3
	A. E. Anglin, MS 106-1	1
	C. E. Lowell, MS 49-1	3
	J. C. Freche, MS 49-1	1
	C. A. Barrett, MS 49-1	1
	G. J. Santoro, MS 49-1	1

Langley Research Center
National Aeronautics and Space Administration
Langley Station
Hampton, Virginia 23365

Attention:	Library	1
	Richard Pride, MS 188A	1

George C. Marshall Space Flight Center
National Aeronautics and Space Administration
Marshall Space Flight Center, Alabama 35812

Attention:	Library	1

NASA Scientific and Technical Information Facility
P. O. Box 3300
College Park, Maryland 20740

Attention:	NASA Representative, RQT-2448	6

Jet Propulsion Laboratory
4800 Oak Grove Drive
Pasadena, California 91103
Attention: Library 1

Ames Research Center
National Aeronautics and Space Administration
Moffett Field, California 94035
Attention: Library 1

Goddard Space Flight Center
National Aeronautics and Space Administration
Greenbelt, Maryland 20771
Attention: Library 1
D. F. Hasson, Code 714 1
C. E. Vest, Code 249.1 1

Manned Spacecraft Center
National Aeronautics and Space Administration
Houston, Texas 77058
Attention: Library 1
N. Chaffee, EB-4 1

Flight Research Center
National Aeronautics and Space Administration
P. O. Box 273
Edwards California 93523
Attention: Library 1

Federal Aviation Agency
800 Independence Avenue, SW
Washington, D. C. 20553
Attention: Brig. Gen. J. C. Maxwell 1
F. B. Howard, SS/210 1

Atomic Energy Commission
Washington, D. C. 20545
Attention: Technical Reports Library 1
Jules Simmons 1

Department of Air Force
Office of Scientific Research
Propulsion Research Division
Washington, D. C. 20525 1

Headquarters
Wright Patterson AFB, Ohio 45433
Attention: MAAM: Technical Library 1
AFSC-FTDS 1
AFML: Dr. A. M. Lovelace 1
SESOS: J. L. Wilkins 1
MAMP: I. Perlmutter 1

Department of the Navy
Office of Naval Research
Code 429
Washington, D. C. 20525
Attention: Dr. R. Roberts 1

Chief, Bureau of Naval Weapons
Department of the Navy
Washington, D. C. 20525
Attention: T. F. Kearns 1

U. S. Army Aviation Materials Laboratory
Fort Eustis, Virginia 23604
Attention: John White, Chief, SMOFE-APG 1

Army Materials Research Agency
Watertown Arsenal
Watertown, Massachusetts 02172
Attention: S. V. Arnold, Director 1

Aerojet-General Corporation
P. O. Box 296
Azusa, California
Attention: I. Petker, Dept. 5127, Bldg. 159 1

American Society for Metals
Metals Park
Novelty, Ohio 44073
Attention: Dr. Taylor Lyman 1

AVCO Lycoming Aircraft
550 South Main Street
Stratford, Connecticut 06497
Attention: W. R. Freeman, Jr. 1

Battelle Memorial Institute
505 King Avenue
Columbus, Ohio 43201
Attention: Defense Metals Information Center 1
Dr. A. Z. Hed 1
Dr. R. I. Jaffee 1
Dr. B. A. Wilcox

Bendix Corporation
Research Laboratories Division
Southfield, Michigan 48075
Attention: C. B. Sung 1

Boeing Company
P. O. Box 733
Renton, Washington 98055
Attention: W. E. Binz, SST Unit Chief 1

Clemson University
College of Engineering
Clemson, South Carolina 29631
Attention: Dr. J. S. Wolf 1

General Electric Company
Advanced Technology Laboratory
Schenectady, New York 12305
Attention: Library 1

General Electric Company
MPTL-AETD
Cincinnati, Ohio 45215
Attention: L. P. Jahnke 1
C. S. Wukusick 1

General Motors Corporation
Allison Division
Indianapolis, Indiana 46206
Attention: K. K. Hanink, Materials Laboratory 1

International Nickel Company
67 Wall Street
New York, New York 10005
Attention: R. R. Dewitt 1

International Nickel Company
P. D. Merica Research Laboratory
Sterling Forest
Suffern, New York 10901
Attention: Dr. F. Decker 1

Lockheed Palo Alto Research Laboratories
Materials and Science Laboratory 52-30
3251 Hanover Street
Palo Alto, California 94304
Attention: E. C. Burke 1

Michigan Technical University
Houghton, Michigan 49931
Attention: Prof. R. W. Guard 1

Ohio State University
Columbus, Ohio 43210
Attention: Dr. A. R. Rapp, Dept. of Metallurgical Engineering 1

Solar Division
International Harvester Corporation
San Diego, California 92112
Attention: J. V. Long, Director of Research 1

Tem-Pres Research, Inc.
1401 South Atherton Street
State College, Pennsylvania 16801 1

United Aircraft Corporation
400 Main Street
East Hartford, Connecticut 06108
Attention: E. F. Bradley, Chief, Materials Engineering 1